Incorporation of the Paleogene foreland into the Neogene Puna plateau: The Salar de Antofalla area, NW Argentina

B. Kraemer [a,*], D. Adelmann [a], M. Alten [a], W. Schnurr [a], K. Erpenstein [b], E. Kiefer [a], P. van den Bogaard [c], K. Görler [a]

[a]*Institut für Geologie, Geophysik und Geoinformatik, Freie Universität Berlin, Malteserstr 74-100, D-12249, Berlin, Germany*
[b]*Sergeomin, Federico Zuarzo 1673, Casilla, 2729, La Paz, Bolivia*
[c]*GEOMAR Forschungszentrum, Wischhofstrasse 1-3, D-24148, Kiel, Germany*

Abstract

This paper presents a detailed tectonosedimentary and volcanic description of the Salar de Antofalla area, along with an evolutionary model of the Southern Puna during the Cenozoic. Cenozoic sedimentation started during the Late Eocene at the climax of the Incaic phase in the Chilean Precordillera. Both playa mud and sandflat as well as fluvial sediments (Quiñoas Formation) of this time are interpreted as deposits of an uniform sedimentation area which was part of a wide retroarc foreland basin east of the Precordillera. Tectonic activity started during the Late Oligocene and is documented by thrust and reverse faulting. Due to thick-skinned deformation, the former coherent part of the foreland basin was subdivided into broken foreland basins filled with alluvial and eolian sediments (Chacras Formation). Their buildup could have been accompanied by the initial uplift and crustal thickening of the Southern Puna. As a consequence of continuing contractional tectonism during Early Miocene, the Salar de Antofalla area was further subdivided into a number of small intra-arc depocenters in which alluvial fan and fluvial sediments (Potrero Grande Formation) were deposited. Several intermediate stratovolcanic centers began to erupt between 18 Ma and 14 Ma. Geochemically, these magmas display an arc signature. They were generated by interaction of basaltic magmas with Andean continental crust thickened to at least 40 km. Reverse faulting and thrusting during the Middle to Late Miocene led to an intra-arc basin filled with thick alluvial fan and evaporite sediments (Juncalito Formation). Since the Late Miocene/Early Pliocene, mainly basaltic andesitic magmas erupted at monogenetic centers located east of the volcanic arc. During the Pliocene, tectonic shortening continued with local strike-slip components. These relief-forming processes reduced the Salar de Antofalla basin to its present narrow and elongated shape and triggered the final alluvial fan sedimentation (Escondida Formation). © 1999 Elsevier Science Ltd. All rights reserved.

Resumen

Dando una detallada descripción tectono-sedimentaria y volcánica del área del Salar de Antofalla, presentamos un modelo de evolución para la Puna Austral durante el Cenozoico. La sedimentación cenozoica comenzó durante el Eoceno superior, en el punto culminante de la fase Incaica de la Precordillera Chilena. Playa con llanura de fango y arena, como también sedimentos fluviales (Formación Quiñoas) de este período, son interpretados como depósitos de un área de sedimentación uniforme, que formaba parte de una amplia cuenca de antepaís de retroarco al este de la Precordillera Chilena. La actividad tectónica comenzó durante el Oligoceno tardío y está documentada por cabalgamientos y fallas inversas. Debido a la deformación del tipo "thick-skinned", la parte coherente de la cuenca de antepaís fue subdividida en una cuenca de antepaís segmentada ("broken-foreland basin") y rellenada con depósitos aluviales y eólicos (Formación Chacras). Su desarrollo estuvo presumiblemente acompañada por un levantamiento inicial y un engrosamiento de la corteza de la Puna Austral. Debido a la continuación del tectonismo de

---

contracción durante el Mioceno temprano, el área del Salar de Antofalla fue sucesivamente dividida en pequeños depocentros de intra-arco, en los cuales fueron depositados abanicos aluviales y sedimentos fluviales (Formación Potrero Grande). Estratovolcanes con magmas de composición intermedia iniciaron su actividad entre los 18 Ma y 14 Ma. Desde el punto de vista geoquímico, estos magmas muestran una signatura de arco volcánico y que ascendieron a través de una corteza con un espesor mínimo de 40 km. En el Mioceno medio a tardío, fallas inversas y cabalgamientos dieron a la cuenca una forma asimétrica. Esta cuenca fue rellenada con sedimentos de abanicos aluviales y gruesos depósitos evaporíticos (Formación Juncalito). Desde el Mioceno tardío/Plioceno temprano comenzó la emisión de andesitas basálticas asociadas a centros monogenéticos detrás del arco volcánico. El acortamiento tectónico continuó durante el Plioceno con fallas de rumbo distribuidas localmente, las cuales redujeron la cuenca del Salar de Antofalla a su actual forma estrecha y elongada y provocó la última deposición de conos aluviales (Formación Escondida).

1. Introduction

The Salar de Antofalla area is situated in the Argentine Puna, the southern part of the Central Andean Altiplano/Puna plateau (Fig. 1). The high plateau is characterized by an average elevation of about 3.65 km above sea level and coincides with an area of crustal thickness of more than 70 km (James, 1971; Wigger, 1988; Isacks, 1988). The Puna alone reaches 4.4 km average elevation, attributed by Whitman et al. (1996) to thinning of the lithosphere. The Altiplano and Puna extend east of the Western Cordillera, the active volcanic arc front of the Central Andean Volcanic Zone (CVZ). The CVZ is related to a region between 15°S and 28°S where the Nazca plate is subducted beneath the South American plate with a moderate slab angle (∼30°) (Barazangi and Isacks, 1976). Farther north and south, the slab angle flattens to a nearly horizontal position and active volcanism is absent. The Southern Puna is situated in the transition at the southern end of the moderate slab-dip zone (Isacks, 1988; Cahill and Isacks, 1992).

The Puna is characterized by a steep local relief caused by contractional "basins and ranges" (Allmendinger et al., 1997), volcanoes, and sluggish erosion due to an arid climate. Examples of basins and ranges in the working area are the Salar de Antofalla and the Salar de Incahuasi basins and the Sierra de
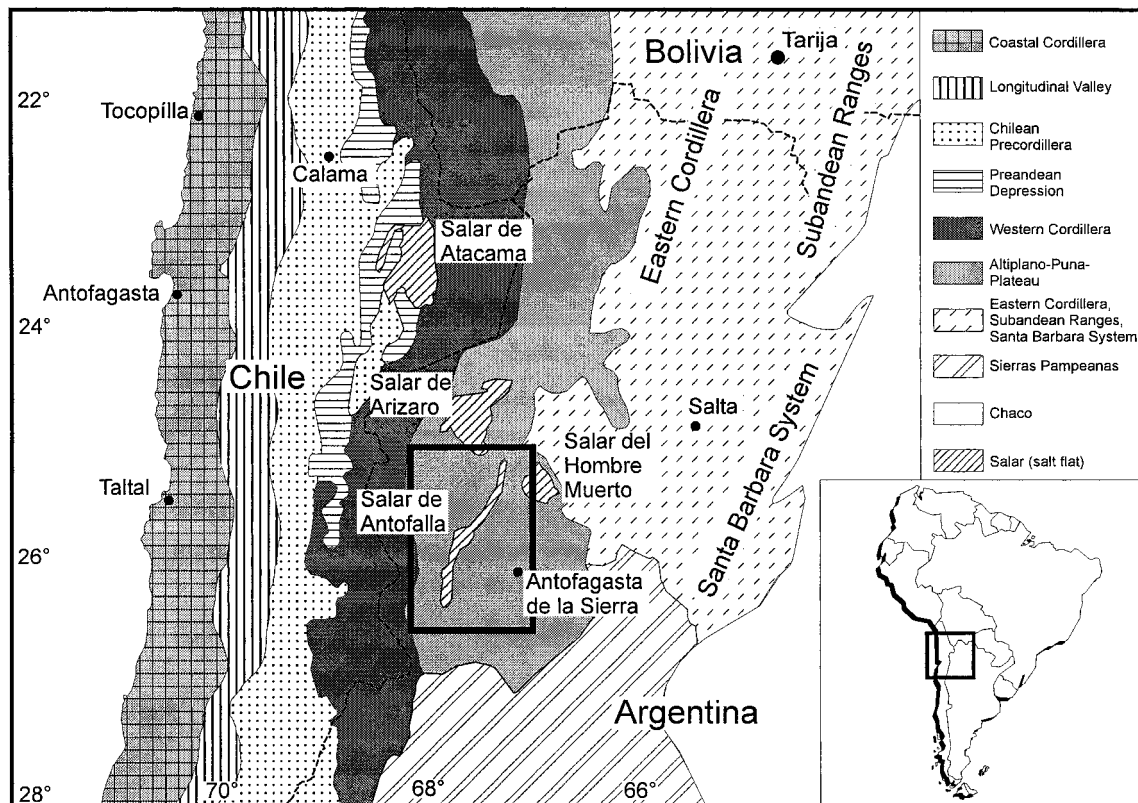

Fig. 1. Location map of the Southern Central Andes with morphostructural units (modified after Reutter et al., 1988 and Jordan and Gardeweg, 1989) and significant salt flats mentioned in this paper.
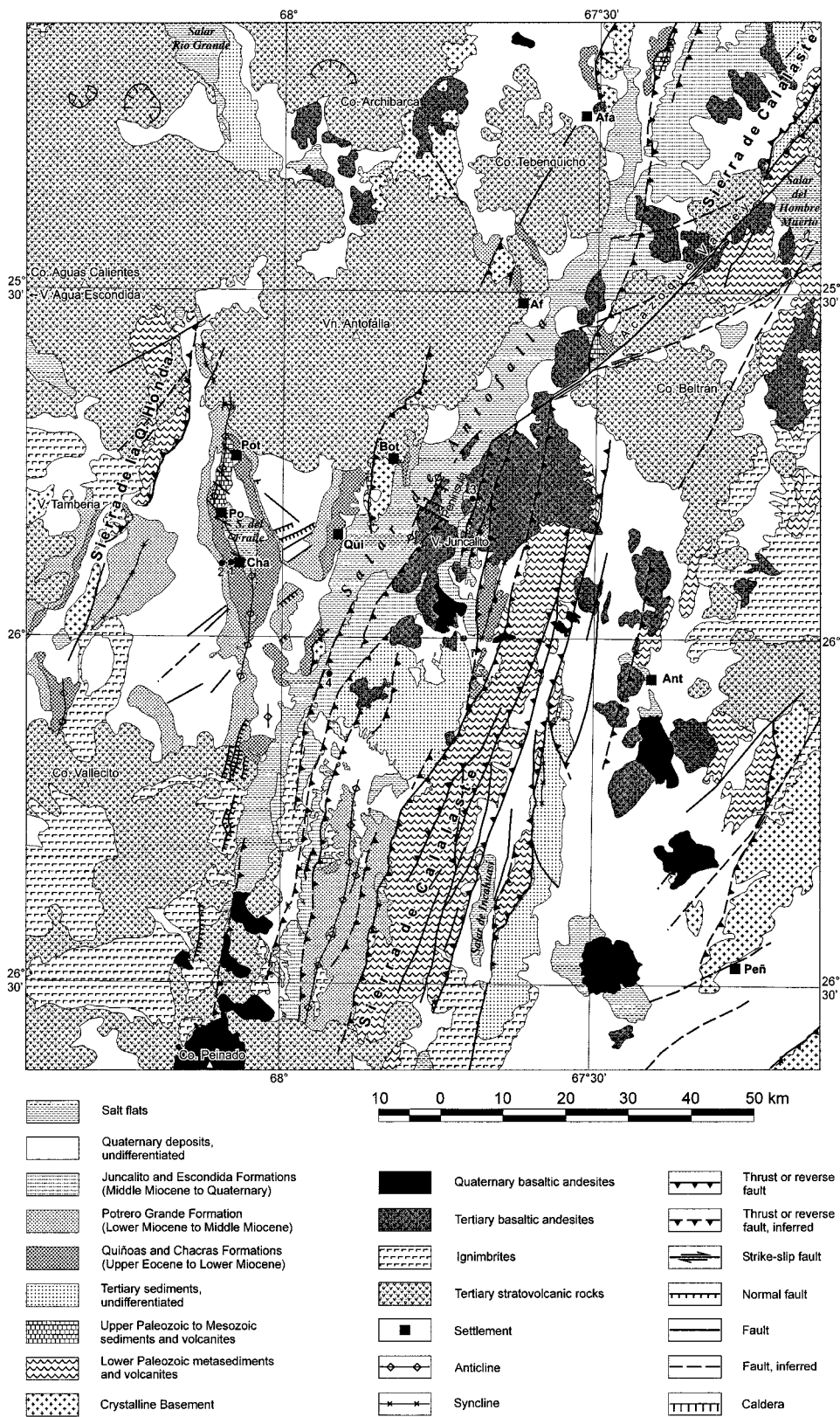
Fig. 2. Geological map of the Salar de Antofalla area, NW Argentina. Black dots refer to stratigraphical logs in Figs. 3, 4, 5 and 6 (1: Quiñoas and Chacras Formations, 2: Potrero Grande Formation, 3: lower part of the Juncalito Formation, 4: upper part of the Juncalito Formation and Escondida Formation). Abbreviations: Af—Antofalla village, Afa-Antofallito, Ant–Antofagasta de la Sierra, Bot—Botijuela, Cha—Las Chacras, Co-Cerro, Peñ—El Peñón, Po—Potrerillo, Pot—Potrero Grande, Qui—Las Quiñoas, Vn-Voleán.

Table 1

Analytical data for K–Ar and $^{40}Ar/^{39}Ar$ ages of magmatic and metamorphic rocks from the Salar de Antofalla area, in stratigraphic order (oldest to youngest) (*: plateau age; **: mean apparent age)

Sample number	Latitude Longitude	Lithology	Dated material	Method	K [%]	^{40}Ar [ppm]	$^{40}Ar/^{40}Ar_{tot}$	No. of analysis	Isochron (MSWD)	$^{40}Ar/^{36}Ar_{initial}$	Age $\pm \sigma$ [Ma]
ID-3	25°47.573 S 67°50.424 W	Migmatic gneiss	Muscovite	K/Ar	9.18	0.300	0.921				419.0 ± 8.0
ID-1	25°47.397 S 67°51.442 W	Granite	Muscovite	K/Ar	9.157	0.2981	0.927				417.0 ± 8.0
ID-37	26°01.288 S 67°56.266 W	Granite	Muscovite	K/Ar	9.016	0.2713	0.930				389.0 ± 8.0
ID-50	26°19.468 S 67°55.799 W	Tuff	Feldspar	K/Ar	11.654	0.2452	0.954				281.0 ± 6.0
ID-94	25°34.062 S 67°29.760 W	Tuff	Kfsp	Ar/Ar				7	4.23	305.0 ± 12	276.0 ± 1.0
ID-67	25°47.332 S 68°06.472 W	Tuff	Biotite	K/Ar	6.671	0.1338	0.811				268.0 ± 6.0
ID-63	25°43.526 S 68°05.604 W	Tuff	Kfsp	Ar/Ar				4	1.88	359.0 ± 13	264.5 ± 1.5
ID-66	25°47.679 S 68°06.250 W	Andesite	Plag	Ar/Ar				1			234.0 ± 1.0**
ID-22	25°46.625 S 67°48.254 W	Porphyr	Whole rock	K/Ar	1.666	0.02597	0.776				212.0 ± 5.0
ID-102	25°47.627 S 68°06.698 W	Porphyritic rhyolith	Feldspar	K/Ar	2.771	0.04021	0.6178				198.0 ± 5.0
ID-23	25°47.358 S 68°05.675 W	Intermediate lava flow	Feldspar	K/Ar	0.889	0.0126	0.369				194.0 ± 6.0
ID-64	25°49.001 S 68°03.800 W	Tuff	Plag	Ar/Ar				10	3.29	304.0 ± 10	37.6 ± 0.3
ID-51	25°53.404 S 68°05.421 W	Tuff	Biotite	K/Ar	4.823	0.009747	0.435				28.9 ± 0.8
ID-6	25°11.590 S 67°30.810 W	Tuff	Amphibole	K/Ar	0.857	0.001449	0.157				24.2 ± 0.9
ID-18	25°58.157 S 68°03.828 W	Tuff	Biotite	K/Ar	4.165	0.006537	0.299				22.5 ± 0.6
ID-40	25°39.427 S 67°48.254 W	Tuff	Biotite	K/Ar	4.816	0.006199	0.214				18.5 ± 0.5
ID-52	25°53.803 S 68°05.421 W	Tuff	Glass	K/Ar	3.778	0.004741	0.292				18.0 ± 0.6
ID-8	25°46.109 S 68°12.003 W	Tuff	Feldspar	Ar/Ar				10	1.9	269.9 ± 2.5	17.39 ± 0.08
ID-97	25°43.329 S 68°03.752 W	Tuff	Plag	Ar/Ar				10	1.76	330.0 ± 16	17.1 ± 0.3
ID-36	25°46.288 S 67°25.542 W	Dacite	Feldspar	Ar/Ar				11	1.1	294.3 ± 0.4	14.1 ± 0.4
ID-20	25°19.771 S 67°58.883 W	Andesite	Feldspar	Ar/Ar				8	1.0	295.4 ± 1.1	12.8 ± 1.2
ID-48	25°48.225 S 67°41.712 W	Pyroclastic rock	Feldspar	Ar/Ar				7	0.9	294.0 ± 2.0	11.2 ± 0.3
ID-26	25°14.117 S 67°39.937 W	Andesite	Feldspar	Ar/Ar				10	2.0	293.6 ± 1.3	11.0 ± 0.5
ID-83	25°28.922 S 67°39.124 W	Ignimbrite (pumice)	Plag	Ar/Ar				10	2.06	300.0 ± 1.0	10.9 ± 0.3
ID-25	25°14.771 S 67°49.346 W	Andesite	Feldspar	Ar/Ar				10	1.7	297.2 ± 0.5	10.7 ± 0.7
ID-47	25°42.818 S 68°04.440 W	Ignimbrite (pumice)	Biotite	Ar/Ar				20	Plateau (3–5.62%)		9.8 ± 0.5*
ID-65	25°43.804 S 68°03.563 W	Ignimbrite (pumice)	Plag	Ar/Ar				3			9.6 ± 0.2**
ID-53	25°07.631 S 67°23.778 W	Tuff	Biotite	K/Ar	7.875	0.005106	0.290				9.3 ± 0.2
ID-91	26°00.549 S 67°54.649 W	Tuff	Plag	Ar/Ar				2			7.9 ± 0.3**
ID-41	25°43.502 S 68°05.876 W	Dacite	Biotite	K/Ar	7.812	0.004155	0.248				7.7 ± 0.2
ID-87	25°44.298 S 67°42.544 W	Andesite	Whole rock	K/Ar	2.075	0.001011	0.042				7.0 ± 0.3
ID-72	26°29.048 S 67°43.012 W	Ignimbrite (pumice)	Biotite	K/Ar	7.819	0.003422	0.186				6.3 ± 0.2
ID-27	25°26.583 S 67°33.849 W	Andesite	Feldspar	Ar/Ar				7	0.6	296.7 ± 1.8	5.96 ± 0.03
ID-46	25°27.821 S 67°20.431 W	Andesite	Whole rock	K/Ar	2.113	0.00078	0.167				5.3 ± 0.3
ID-42	25°55.772 S 67°49.319 W	Basaltic andesite	Whole rock	K/Ar	1.197	0.000436	0.075				5.2 ± 0.3
ID-56	25°31.742 S 67°35.280 W	Andesite	Plag	Ar/Ar				4	3.05	304.0 ± 53	4.8 ± 0.5
ID-30	25°48.742 S 67°35.107 W	Basaltic andesite	Glass	Ar/Ar				9	1.7	295.0 ± 1.0	4.68 ± 0.08
ID-17	25°59.520 S 67°52.027 W	Monogenetic mafic flow	Whole rock	K/Ar	1.708	0.000543	0.074				4.6 ± 0.2
ID-35	25°49.845 S 67°44.834 W	Tuff	Whole rock	K/Ar	2.840		0.130				4.6 ± 0.5
ID-13	26°10.860 S 68°03.246 W	Andesite	Plag	K/Ar	8.473	0.001893	0.347				3.61 ± 0.02
ID-11	26°14.669 S 67°57.976 W	Ignimbrite (matrix)	Feldspar	K/Ar	3.609	0.000430	0.052				3.605 ± 0.005
ID-16	26°00.042 S 67°51.293 W	Tuff	Sanidine	Ar/Ar				9	1.6	289.0 ± 9.0	3.2 ± 0.1
ID-73	26°17.315 S 67°35.647 W	Tuff	Glass	Ar/Ar				9	0.3	289.0 ± 9.0	1.7 ± 0.01
ID-33	25°47.770 S 67°42.548 W	Tuff	Biotite	Ar/Ar				7	0.9	303.6 ± 8.2	0.47 ± 0.01
ID-71	26°31.762 S 67°42.668 W	Ignimbrite (pumice)	Feldspar	K/Ar	5.507	0.000072	0.040				0.2 ± 0.1
ID-9	26°24.487 S 68°04.772 W	Basaltic andesite	Glass	Ar/Ar				7	1.8	298.0 ± 4.0	0.2 ± 0.09

Calalaste range (Fig. 2). The ranges are mostly composed of deformed Paleozoic rocks. The endorheic basins in between are filled with Miocene to Recent halite-dominated evaporites unconformably overlying Late Eocene to Miocene molasse-like, continental clastics. Miocene and younger volcanic centers of the Puna are located at several NW-trending lineaments (Salfity, 1985). Examples in the Salar de Antofalla area are the Cerro Beltrán and the Volcán Archibarca.

Tectonically, the ranges were affected by thrusting and folding prior to and contemporaneous with Middle and Late Miocene subsidence of the adjacent basins (Allmendinger et al., 1997). Deformation of the ranges continued to the Pliocene (Marrett et al., 1994; Allmendinger et al., 1997). Signs of younger deformation of alluvial fans and young volcanites are rare and crustal seismicity is low, except at the northern and southern ends of the high plateau (Wigger, 1988; Allmendinger et al., 1997). East of the Puna, the Eastern Cordillera arises, mainly composed of Precambrian rocks and minor Late Cretaceous deposits. In the Santa Bárbara System and the Sierras Pampeanas, contiguous to the Eastern Cordillera to the east, Precambrian metamorphic rocks as well as Paleozoic plutonic and sedimentary rocks are overlain by Cretaceous and Tertiary sediments. They were affected by thick-skinned compressive deformation during the Andean orogeny (Allmendinger et al., 1983; Willner et al., 1987, Alonso et al., 1991).

The mechanism and timing of crustal thickening and uplift of the Central Andean plateau are currently under discussion (Isacks, 1988; Francis and Hawkesworth, 1994; Allmendinger et al., 1997; Lamb et al., 1997). In a comprehensive review of the available geological data, Allmendinger et al. (1997) refined the model of plateau evolution given by Isacks (1988) and showed that plateau evolution differs between the Altiplano and Puna segments. They suggested that the Puna began to rise between 15 and 20 Ma due to tectonic shortening distributed across the width of the plateau. According to Kay et al. (1994a) and Allmendinger and Gubbels (1996), crustal shortening of the Puna continued locally until 1–2 Ma and was accompanied, in the southern part, by lithospheric delamination.

However, few studies on the Cenozoic basin evolution of the Puna have been carried out which give information about the deformational history and mechanism. A comprehensive review of basin evolution in the Central Andes (20–28°S) was given by Jordan and Alonso (1987). They postulated a wide post-Incaic (40–25 Ma) foreland basin east of the Incaic deformation front. In their opinion, the Neogene magmatic arc appeared between 25–10 Ma to the west of this basin and sedimentation continued in the east without major tectonic activity in the Southern Puna. For the last 10 my, they envisaged that the effects of the Quechua and Diaguita phases established different depocenters in the former uniform basin (Jordan and Alonso, 1987). Alonso et al. (1991) suggested that "playa conditions" began in the Puna at 15 Ma and sedimentation of evaporites at 7–8 Ma. Vandervoort et al. (1995) proposed a time frame of 24.2–14.1 Ma for the initiation of the isolated basins. They concluded that this may have coincided with the beginning of contractional tectonism and the uplift of the Puna due to tectonic crustal thickening.

In the Southern Puna, Alonso et al. (1991) and Vandervoort et al. (1995) were hindered by the lack of sufficient radiometric and biostratigraphical age data especially for the sedimentary section older than 15 Ma. To get a more complete view of the geological history and plateau building in the Southern Puna, we present tectonic, magmatic, and sedimentary data on Paleozoic to Cenozoic rocks of the Salar de Antofalla area. Based on mineral and whole rock $^{40}Ar/^{39}Ar$ and K–Ar analyses, we also have obtained more than 70 new radiometric ages. A selection of 46 ages is given in Table 1. Based on the age data, we improve the temporal resolution of geological events in the Southern Puna especially during the Cenozoic. Combining facies, structural, and geochemical data of the Cenozoic sedimentary record and volcanic rocks, we present a modified model of foreland segmentation and plateau evolution.

2. Stratigraphy and facies

The Cenozoic sedimentary basins and related volcanic belts of the Southern Puna formed on a continental crust which is composed of Precambrian to Early Paleozoic crystalline basement rocks and Lower Paleozoic strata as well as Permian and Mesozoic rocks. A fivefold division of the Cenozoic, whose oldest sediments have a Late Eocene age, is evident in the Salar de Antofalla area.

2.1. Crystalline basement

Crystalline basement rocks are exposed along the western margin of the Salar de Antofalla associated with reverse faults (Voss, in preparation), west and southwest of the volcano Tebenquicho, south of the Sierra de la Quebrada Honda, and at the southwestern border of the Sierra de Calalaste (Fig. 2). Migmatic gneisses and metabasites, penetrated by several generations of granitoids and aplites, prevail. Age determinations on a migmatic gneiss yielded 419.0 ± 8.0 Ma (ID-3) (for age data see Table 1) and on two granite samples 417.0 ± 8.0 Ma (ID-1) as well as 389.0 ± 8.0 Ma (ID-37). The Archibarca granite, located in the

NW of the study area (Fig. 2), has an Early Paleozoic age of 485.0 ± 15.0 Ma (Palma et al., 1986).

Intensely deformed phyllites and metagraywackes occur in tectonic contact with high-grade metamorphic rocks northeast of the Vega Quiñoas (Fig. 2). Based on lithological similarities we consider them as an equivalent to the Late Precambrian Puncoviscana Formation which crops out in widespread areas of NW Argentina (Aceñolaza et al., 1988).

2.2. Lower Paleozoic sediments and volcanites

Among the most common rocks forming the Andean basement east of the Salar de Antofalla are low-grade metasediments with intercalated metabasites of Early Paleozoic age. The sedimentary suite is represented by a thick alternation of mostly turbiditic sandstones and siltstones. Common features are Bouma cycles, sharp erosional contacts, flute casts, and tool marks. The rock age is not well defined. In the Salar del Hombre Muerto area (Fig. 1), a graptolite assemblage indicates a Middle to Late Ordovician age (Aceñolaza et al., 1975). Due to lithological and facies similarities, these rocks may be an analogue of Ordovician sediments of the Northern Puna which Bahlburg (1990) interpreted as deep water sediments deposited in a backarc basin.

2.3. Upper Paleozoic and Mesozoic sediments and volcanites

North of the Vega Quiñoas (Fig. 2), the crystalline basement is nonconformably overlain by unmetamorphosed siliciclastic sediments of Permian age (Voss et al., 1996). They are composed of a coarse basal conglomerate, derived from the crystalline basement, followed by an alternation of large-scale cross-bedded quartz sandstones and quartz conglomerates, probably representing a beach environment. In the Salina del Fraile area, an approximately 200 m thick succession of playa/sebkha siltstones and eolian sandstones overlain by an alternation of quartz sandstones and reddish siltstones of a presumably littoral environment is exposed. Petrified fragments of stigmaria root of *Lepidodendron* or *Sigillaria* indicate a Late Carboniferous to Early Permian age (D. Vogellehner, personal communication). Interbedded tuff layers yielded ages of 268.0 ± 6.0 Ma (ID-67), 276.0 ± 1.0 Ma (ID-94) and 264.5 ± 1.5 Ma (ID-63). Another age [281.0 ± 6.0 Ma (ID-50)] from a tuff layer from the southeastern margin of the Salar de Antofalla indicates the widespread occurrence of Permian sediments in the study area.

In the Salina del Fraile area, the Permian strata are cut by dikes of intermediate composition of Triassic age (Voss et al., 1996) [212.0 ± 5.0 Ma (ID-22),

234.0 ± 1.0 Ma (ID-66)]. The Permian is unconformably overlain by a more than 100 m thick alternation of marls and sandstones with pillow lavas and hyaloclastite breccias at its base and other intercalated lava beds of an Early Jurassic age (Voss et al., 1996) [198.0 ± 5.0 Ma (ID-102), 194.0 ± 6.0 Ma (ID-23)]. Interbedded are coquina beds and oolithic limestones. Remnants of foraminifera (*Psammosphaera* sp.), cyanophyta (*Rivularia* sp.), ostracodes, and echinoderms have been found. These fossils and the occurrence of a 2 m thick magnetite placer bed hint towards a deposition in a littoral to shallow marine environment.

2.4. Upper Eocene to Upper Oligocene (Quiñoas Formation)

The Late Eocene to Late Oligocene strata defined by Voss (in preparation) as the Quiñoas Formation are more than 750 m thick and consist of reddish, sometimes gypsiferous pelites and sandstones locally with conglomeratic intercalations. The succession shows variations in facies and lithology which allow a subdivision into two members (Fig. 3).

The base of the Quiñoas member I is exposed north of the Vega Quiñoas (Fig. 2) and shows an erosional contact with the underlying pre-Cenozoic rocks. It consists of red conglomerates containing pebbles of phyllites, granites, and schists which originated from the crystalline basement. The remaining part of the first member is dominated by an alternation of siltstones and fine-grained sandstones, rarely interbedded with lenticular bodies of conglomerates. The siltstones show horizontal lamination, bioturbation, and desiccation cracks. Thin gypsum layers are occasionally intercalated. The sandstones display a relatively uniform thickness over a large lateral extent, asymmetrical current-ripples, and erosive basal surfaces. Locally, they are pebbly and contain horizons of mudclasts. Lithology and sedimentary features indicate a deposition in periodically flooded playa sand and mudflats.

Member II is dominated by medium- to fine-grained sandstones reaching a thickness of 300 m (Fig. 3). They are massively bedded on a scale of 0.5–5.0 m, with a planar or erosive lower contact. Sedimentary structures are delineated by the presence of mudstone intraclasts and scattered pebbles as well as low-angle trough cross-bedding at the base and horizontal parallel laminae towards the top of the beds. Based on their sedimentary features, we interpret them as deposits of a fluvial distributary system.

In the Quiñoas Formation, unequivocal paleoflow indicators are missing. Paleotransport directions and sedimentary structures for coeval strata in surrounding areas are not available. The only indication for the paleotransport direction was given by Jordan and Alonso (1987) who pointed out that the Oligocene red

beds are more conglomeratic in the west than in the east of the Puna. They assumed that an Incaic mountain belt located in central and western Chile supplied the detritus which was shed eastward to a broad alluvial plain.

Intercalated tuff layers indicate the Late Eocene to Late Oligocene age of the Quiñoas Formation. The oldest dated sediments of member I occur at the eastern margin of the Salina del Fraile, but the base is not exposed. A tuff bed in the deepest portion of this section yielded an age of 37.6 ± 0.3 Ma (ID-64). From another tuff bed near the top of member II an age of 28.9 ± 0.8 Ma (ID-51) has been obtained. The succession is unconformably overlain by conglomerates of the Chacras Formation with a maximum age of 24.2 ± 0.9 Ma (ID-86). Based on its lithological composition, the Quiñoas Formation is possibly correlative to the Geste Formation of the Pastos Grandes and Arizaro areas as described by Turner (1960), Donato (1987) and Alonso (1992).

2.5. Upper Oligocene to Lower Miocene (Chacras Formation)

The Chacras Formation is composed of conglomerates and pebbly sandstones as well as medium- to fine-grained sandstones unconformably overlying member II of the Quiñoas Formation. In the Salina del Fraile area, the succession reaches a thickness of about 350 m (Fig. 3), whereby west of Antofalla village more than 600 m are exposed. The conglomerates are massive, poorly sorted, matrix- to clast-supported, and form laterally continuous sheets. Basal bedding contacts are erosional. Pebbles display diameters of up to 0.5 m, are subangular, and originated from the crystalline basement as well as Lower Paleozoic strata. The nature of the conglomerates suggests a deposition in an alluvial fan environment close to the source areas.

The uppermost part of the Chacras Formation is dominated by medium- to fine-grained sandstones. They display trough cross-stratification with sets 0.5–10.0 m thick, bounded by curved erosion surfaces with a wedge-like appearance. Foreset dips vary between 15° and 25°, declining to around 5° at the base. High-angle trough cross-bedding, grain size characteristics, and excellent sorting correspond to modern eolian dunes (e.g. Hunter, 1977).

West of the actual Salar de Antofalla, imbricated pebbles of the alluvial fan sediments indicate a flow direction towards the west. In contrast, paleoflow indicators measured east of the actual salar show a general transport towards the east. Most likely, the deposits of the Chacras Formation are derived from the erosion of crystalline basement and Early Paleozoic rocks in the area of the present Salar de Antofalla, which were exposed due to relief-forming contractional tectonism
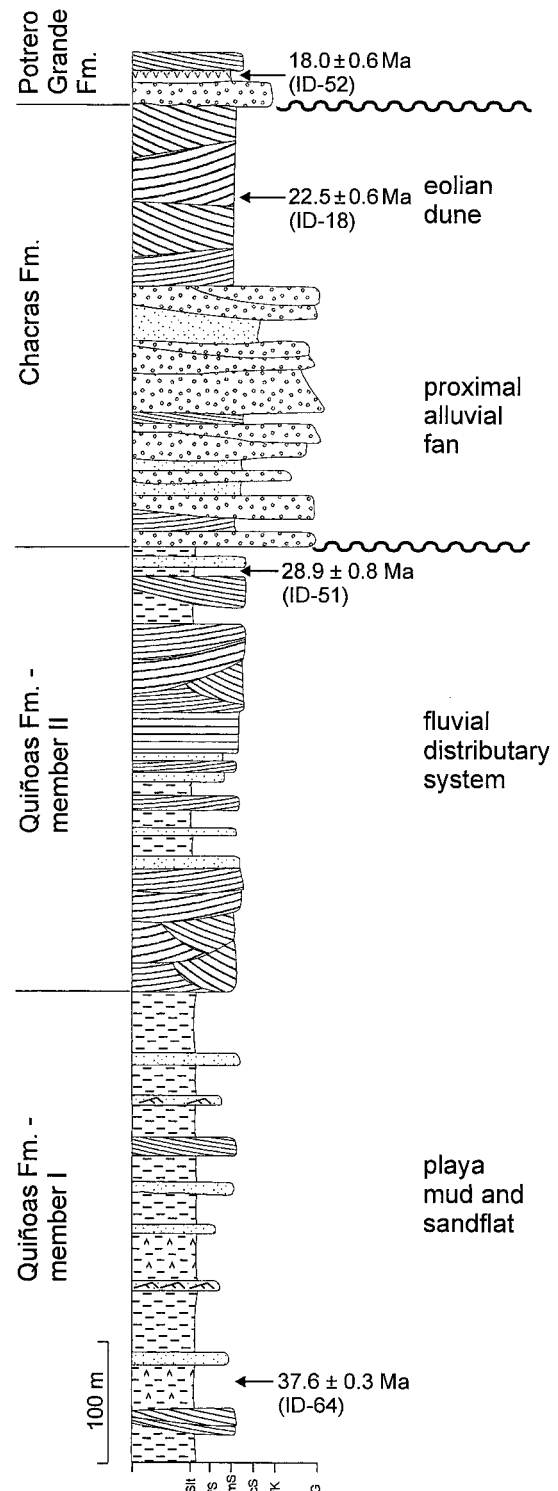

Fig. 3. Stratigraphic column of the Quiñoas and Chacras Formations. Location is shown on Fig. 2. The base of the Quiñoas Formation is not documented in this locality. The contacts between Quiñoas and Chacras Formations as well as between Chacras and Potrero Grande Formations are marked by angular unconformities. For legend see Fig. 4.

during the Late Oligocene (deformation interval D1, see below).

The Late Oligocene to Early Miocene age of the Chacras Formation is evidenced by intercalated tuff layers. The oldest age data was obtained from a tuff bed sampled north of Antofallita [24.2 ± 0.9 Ma (ID-86)]. East of the Salina del Fraile, a tuff yielded an age of 22.5 ± 0.6 Ma (ID-18). The sediments of the Chacras Formation are unconformably overlain by volcaniclastic sediments of the Potrero Grande Formation whose maximum age is dated at 18.0 ± 0.6 Ma (ID-52) (Fig. 3).

2.6. Lower Miocene to Middle Miocene (Potrero Grande Formation)

The Early to Middle Miocene Potrero Grande Formation (Voss, in preparation) unconformably over-lies the deposits of the Chacras Formation. The thickness of the Potrero Grande Formation varies from 50 m near Quiñoas to more than 250 m towards the west in the Salina del Fraile area. Its lithology is characterized by conglomerates composed of volcanic fragments, intercalated fallout tuff layers, and ignimbrites indicating substantial synsedimentary volcanic activity (Fig. 4).

Sedimentation started with conglomerates and conglomeratic sandstones locally reaching a maximum thickness of about 100 m. Volcanic fragments prevail with diameters up to 1.5 m. Pebbles of the Eocene–Oligocene strata, Lower Paleozoic sediments and crystalline basement rocks are of subordinate frequency. The matrix- to clast-supported conglomerates exhibit erosional basal contacts, channelling, and partial pebble imbrication, and are interpreted as proximal alluvial fan sediments. Greyish sandstones and siltstones interbedded with conglomerates follow upsection. Sedimentological features such as medium-scale trough cross-bedding, erosive basal contacts, and channelling indicate a deposition in a fan-related fluvial system.

Paleocurrent directions measured on imbricated pebbles of coarse-grained alluvial fan deposits show significant variations indicating a subdivision into several narrow, separate basins (Fig. 7). This separation was mainly controlled by another interval of contractional tectonism (D2) during the Early Miocene (see below). A west-vergent reverse fault system at the western margin of the present Salar de Antofalla provides clear evidence for this tectonic phase (Voss, in preparation). Here, progressive angular unconformities in the basal Potrero Grande conglomerates (Fig. 9) exhibit the synsedimentary displacement of the fault system. In contrast, paleocurrent measurements in imbricated conglomerates in the Salina del Fraile area indicate a main transport from the west, probably with the Sierra de la Quebrada Honda area as source (Voss, in prep-aration). North of the Salina del Fraile, the Antofalla stratovolcano complex is considered as another source area due to observed flow directions towards the south (Fig. 7).

Locally, thick ignimbrites and volcanic ash layers are intercalated. The oldest tuff beds of the Potrero Grande Formation of the Salina del Fraile area yielded ages of 18.5 ± 0.5 Ma (ID-40) and 18.0 Ma ± 0.6 (ID-52). Age determinations of other interbedded tuff layers and ignimbrites confirm the Miocene age. The youngest samples are ignimbrites from the top of the Potrero Grande Formation near the Salina del Fraile which yielded ages of 9.6 Ma ± 0.2 (ID-65) and 9.8 Ma ± 0.5 (ID-47).

2.7. Middle Miocene to Pliocene (Juncalito Formation)

The Middle Miocene to Pliocene Juncalito Formation unconformably overlies the older Tertiary units and is exposed only at the eastern border of the recent Salar de Antofalla. Two major facies associations can be defined: a coarse-grained alluvial fan facies dominating the lower part of the Juncalito Formation (Fig. 5) and a pelitic/evaporitic playa facies prevailing in the upper part (Fig. 6).

The alluvial fan deposits are characterized by conglomerates interbedded with pebbly sandstones. They reach a thickness of several hundred meters. The conglomerates contain mainly clasts of Quiñoas sandstones as well as Lower Paleozoic metasediments and metavolcanics which originated from the adjacent Sierra de Calalaste area (Fig. 2). Also, fragments of the crystalline basement as well as andesite and dacite clasts are observed. The alluvial fan deposits are thought to be the products of relief-forming processes due to reverse faulting and thrusting during the deformation interval D3 (see below). Paleocurrent measurements indicate a transport mainly from a source area in the east, presumably the Sierra de Calalaste area (Fig. 7).

The playa deposits represent different subenvironments such as mudflats, sandflats, lakes, and saltpans. Most typical features of the mud and sandflat deposits are reddish sandstones and siltstones. Low-angle cross-bedding, desiccation cracks, interbedded gypsum and halite layers are common. Sheet geometry, large lateral extent, and relatively uniform thickness suggest a prevailing deposition as distal sheetflows. Saltpan sediments consisting of alternating millimeter- to decimeter-scale layers of halite and mud are intercalated in the playa mud and sandflat deposits. They were deposited in saline lakes, which produced successive layers of salt through repeated flooding and subsequent reprecipitation. In the central part of the basin, massive halite reaches a thickness of 50 m.

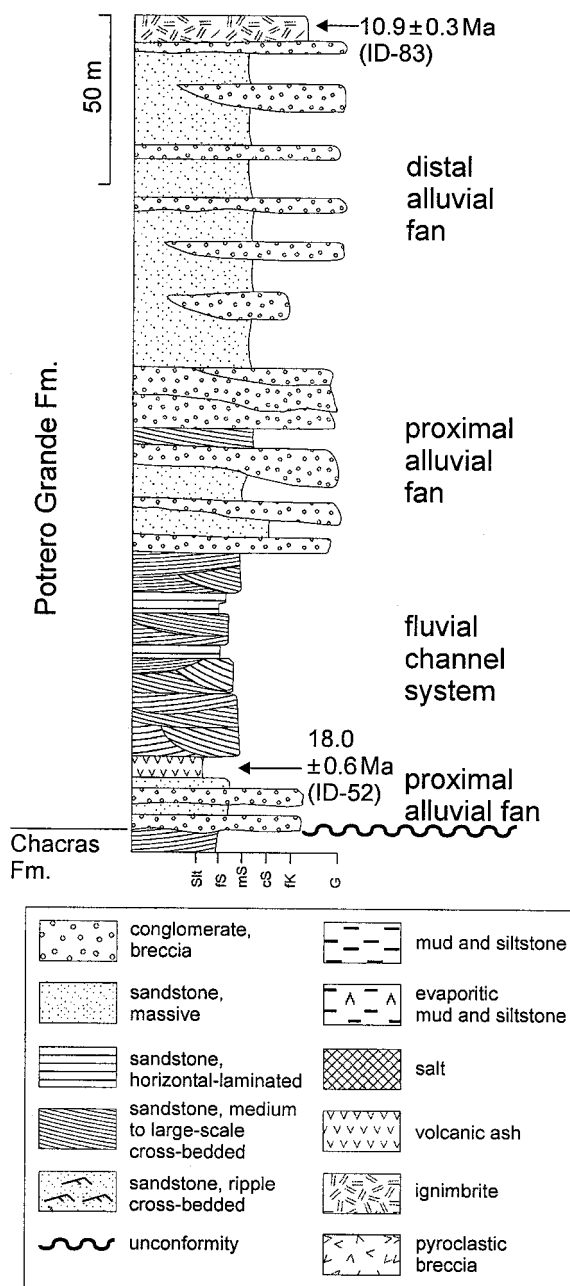Lacustrine sediments were deposited in marginal

Fig. 4. Stratigraphic column of the Potrero Grande Formation overlying the Chacras Formation presented in Fig. 3. Location is shown on Fig. 2. Note the contact to the underlying Chacras Formation marked by an angular unconformity. Sample ID-83 originates from Potrero Grande formation outcropping near Antofalla village.

parts of the basin. They consist of gypsum horizons, grey marls, and white limestones with frequent stromatolites, pisolites, and oolites. Their widespread occurrence in the middle part of the section is thought to be linked to a stage of relative tectonic quiescence and relief equilibration (Adelmann, 1997).

The base of the Juncalito Formation is marked by high diachronism. While deposition of the Potrero Grande Formation in the Salina del Fraile area contin-

ued until 10 Ma, sedimentation of the Juncalito Formation in the Salar de Antofalla area started at about 11–12 Ma. This age is indicated by intercalated pyroclastic rocks. At the base of the exposed section, a brecciated pyroclastic layer, possibly a lahar deposit, yielded an age of 11.2 ± 0.3 Ma (ID-48) (Fig. 4). From other tuffs higher upsection, ages of 9.3 ± 0.2 Ma (ID-53), 7.9 ± 0.3 Ma (ID-91), and 4.6 ± 0.5 Ma (ID-35) were obtained. Age equivalence and lithological similarities permit a correlation of the Juncalito Formation with the Sijes Formation of the Pastos Grandes and Arizaro areas described by Turner (1960) and Alonso et al. (1991).

2.8. Pliocene to Quaternary (Escondida Formation)

The final sedimentation (Escondida Formation, Voss, in preparation) is marked by the abundance of coarse-grained conglomerates unconformably overlying the Juncalito strata (Fig. 6).

The conglomerates are massive and poorly sorted. They are both matrix- and clast-supported and form laterally continuous sheets and channel-like bodies, respectively. Basal bedding contacts are mostly erosional. Based on the sedimentary features, a deposition in a proximal alluvial fan environment is proposed. A maximum thickness of several hundred meters is reached directly at the border of the Sierra de Calalaste, whereas in more distal parts, the average thickness is about 30–50 m (Fig. 6). The clasts are subangular to angular, and reach diameters up to 1.0 m. The composition is similar to those of the Juncalito Formation. Paleocurrent measurements also indicate a main transport from a source area in the east, the Sierra de Calalaste (Fig. 7). Its uplift along extended reverse fault and thrust systems was connected to the final shortening D4 (see below). Due to ongoing synsedimentary compressional deformation, the coarse-grained sediments of the Escondida Formation show some angular unconformities internally.

The oldest sediments of this succession were tectonically affected. Intercalated tuffs yielded an age of 3.605 ± 0.005 Ma (ID-11) and 3.2 ± 0.1 Ma (ID-16). For one of the unaffected fan bodies we obtained an age of 0.47 ± 0.01 Ma (ID-33). Based on lithostratigraphic comparisons, we consider the Escondida Formation as an equivalent to the Batín Formation of the Arizaro area (Donato, 1987) and the Singuel Formation of the Pastos Grandes area (Alonso and Gutiérrez, 1986).

3. Cenozoic deformational history

The Cenozoic deformation in the Salar de Antofalla area is summarized in Fig. 16. Four main stages can
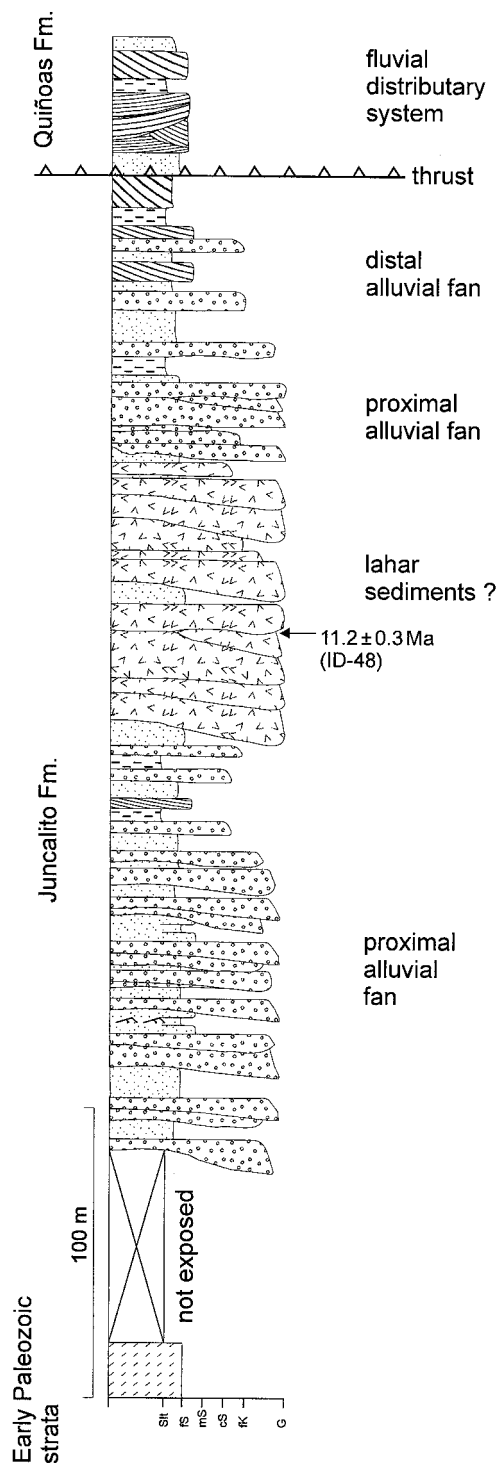
Fig. 5. Stratigraphic column of the lower part of the Juncalito Formation. Location is shown on Fig. 2. For legend see Fig. 4.
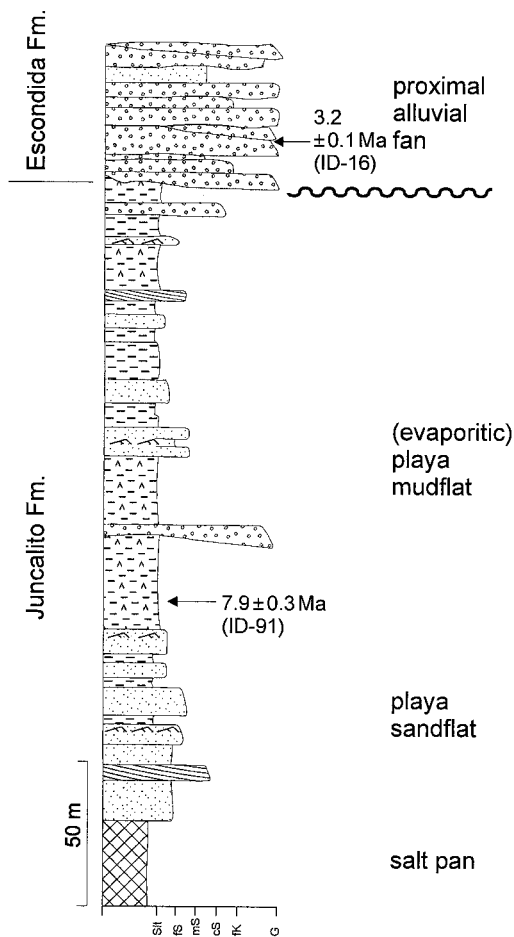

Fig. 6. Stratigraphic column of the upper part of the Juncalito Formation and the lower part of the Escondida Formation. Location is shown on Fig. 2. Note the coarse-grained alluvial fan sediments of the Escondida Formation unconformably overlying the playa mud and sandflat deposits of the Juncalito Formation. For legend see Fig. 4.

be distinguished in general terms and will be discussed below.

During the Late Eocene (~38 Ma, e.g., Döbel et al., 1992) strong contractional to transpressional deformation took place in the Late Cretaceous–Paleogene magmatic arc, the present Chilean Precordillera. The Incaic phase (Steinmann, 1929) triggered east and west-vergent thrusting and reverse faulting of basement blocks onto folded Late Eocene strata. Contraction was accompanied by dextral, arc-parallel strike-slip movements. At the western border of the Precordillera, shortening reached a maximum amount of 32%, becoming less important in the central zone (max. 18%) (Günther et al., 1998).

In the study area, tectonic structures coeval with the Incaic shortening are absent. However, Tertiary sedimentation began simultaneously with tectonism in the Chilean Precordillera. Therefore, we presume that deformation, uplift, and erosion of the Incaic mountain range triggered the sedimentation of the Late Eocene to Late Oligocene Quiñoas Formation.

3.1. Late Oligocene (28–25 Ma, interval D1)

The first deformation involves E–W to WNW–ESE shortening accommodated by a significant west-vergent reverse fault system. The related structures can be
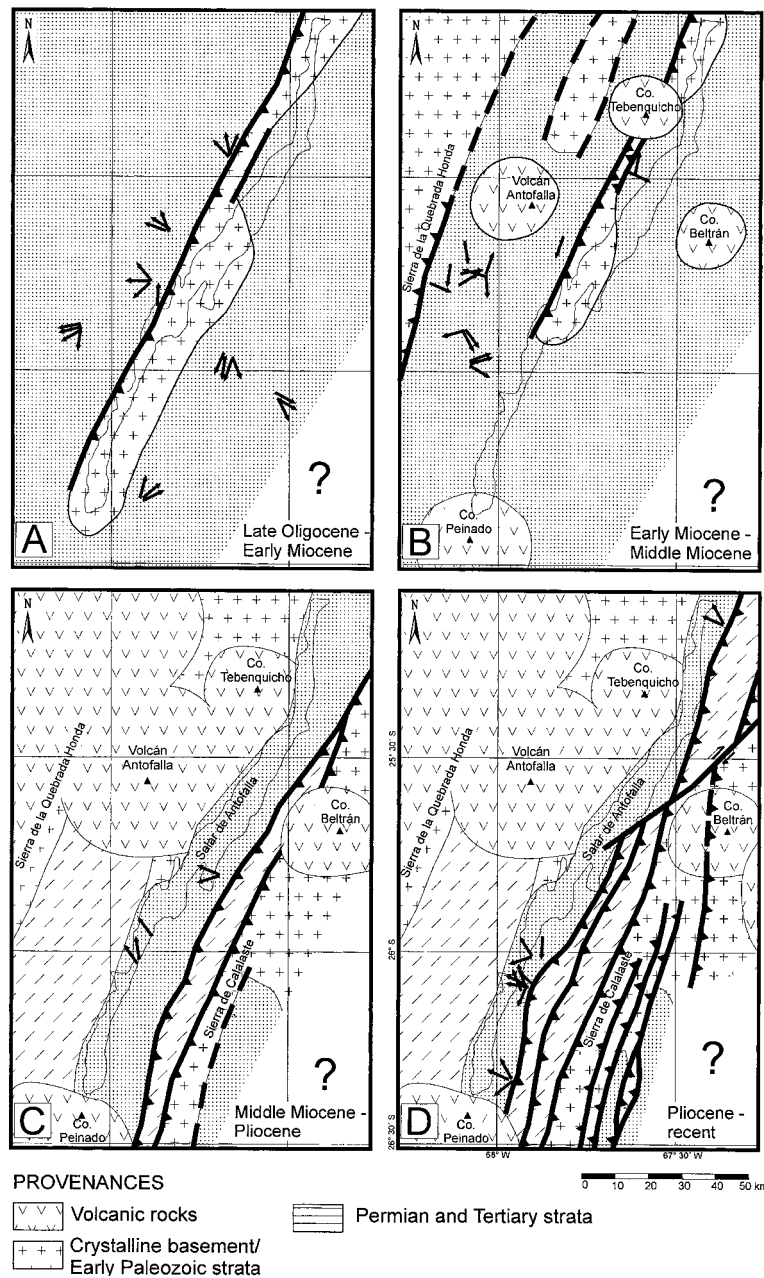
Fig. 7. Presumed distribution of source and sedimentation areas (dotted) based on sediment thicknesses, facies distribution, paleotransport data and clast composition. The arrows show the transport direction measured on imbricated pebbles of coarse-grained alluvial fan deposits. For orientation, the outline of the actual Salar de Antofalla is given. (a) Late Oligocene–Early Miocene (Chacras Formation): The former uniform sedimentation area has been subdivided by uplift of a crystalline basement block. Its western margin was bounded by an extended reverse fault system. Along the fault contact the Chacras sediments are dominated by conglomerates of a proximal alluvial fan environment reaching thicknesses of 200 (north of Antofallita village), 350 m (Las Chacras) and 600 m (west of Antofalla village). Due to a decreased coarse clastic input (Adelmann, in preparation), the eastern margin of the highland is thought to be tectonically passive. (b) Early Miocene–Middle Miocene (Potrero Grande Formation): East and west-vergent reverse faults led to further basement uplift and segmentation of the basin. Several narrow fault-bounded depocenters with presumably N–S orientation developed. The basin configuration was modified by the initial development of stratovolcano complexes (e.g., Antofalla, Beltrán, Tebenquicho). (c) Middle Miocene–Pliocene (Juncalito Formation): Thrust-related frontal ramps produced topographic highs in the Sierra de Calalaste area and led to the development of a narrow, elongate basin in the area of the actual Salar de Antofalla. Mainly Permian and Tertiary sediments, as well as Early Paleozoic metasediments, and subordinate crystalline basement were eroded and shed into the basin. While the eastern basin flank was fault-bounded, the western margin presumably was tectonically passive and formed a flat upland. Concomitantly, in the Salar de Incahuasi area another depocenter developed. (d) Pliocene–Recent (Escondida Formation): Further reverse faulting and thrusting at the eastern edge of the Salar de Antofalla reduced the Salar de Antofalla to its narrow, elongate shape. Syntectonically, coarse-grained alluvial fan sediments were shed from the adjacent Sierra de Calalaste westward into the basin.

observed along the entire western margin of the present Salar de Antofalla where crystalline basement rocks were synsedimentarily reverse faulted and thrust onto tilted Eocene/Oligocene sediments (Fig. 8). Thick-skinned compressive deformation was accompanied by the onset of coarse-grained alluvial fan sedimentation of the Chacras Formation. Directly at the fault contact, west of the thrust front, the conglomeratic part of the succession reaches its highest thickness and highest clast sizes. Transport direction (Fig. 7) as well as clast composition and facies distribution (Adelmann, in preparation; Voss, in preparation) indicate that in the entire area of the present Salar de Antofalla a highland mostly composed of crystalline basement rocks was uplifted.

Deformation D1 is marked by a widespread angular unconformity (max. 30°) between the Quiñoas and the Chacras Formations. Directly beneath the unconformity, a tuff layer yielded an age of 28.9 ± 0.8 Ma (ID-51). The oldest sediments of the overlying Chacras Formation have been dated at 24.2 ± 0.9 Ma (ID-86) and 22.5 ± 0.6 Ma (ID-18). Therefore, we presume that deformation D1 occurred between 28 and 25 Ma.

3.2. Early Miocene (20–17 Ma, interval D2)

During the Early Miocene, renewed E–W to WNW–ESE shortening (D2) reactivated the west-vergent fault system that was active during deformation interval D1. Additionally, D2 produced new reverse faults and thrusts where basement blocks were thrust towards both east and west onto tilted Tertiary strata. Based on the following structures, we suggest that deformation D2 took place between 20 and 17 Ma.

1. At the western border of the present Salar de Antofalla, a west-vergent reverse fault system is exposed. We presume reactivation of the fault system mentioned above (D1 deformation). Associated structures are best displayed east of Volcán Antofalla. There, crystalline basement rocks were reverse faulted onto fan sediments (18.5 ± 0.5 Ma [ID-40]) showing progressive angular unconformities (Fig. 9). Based on these observations, deformation and alluvial fan sedimentation are thought to have occurred coevally.
2. At the eastern margin of the Sierra de la Quebrada Honda, the east-vergent thrusting of Early Paleozoic metasediments onto deposits of the Potrero Grande Formation (17.39 ± 0.08 Ma [ID-8]) is exposed (Voss, in preparation). The latter were presumably syntectonically shed from the Sierra de la Quebrada Honda area indicated by transport direction (Fig. 7) and clast composition.
3. The distinct angular unconformity between the Chacras and Potrero Grande Formations constrains

the time of deformation. In the area of the Salina del Fraile, deformation started after 22.5 ± 0.6 Ma (ID-18, Chacras Formation) and terminated before 17.1 ± 0.3 Ma (ID-97, Potrero Grande Formation).

3.3. Middle Miocene (12–10 Ma, interval D3)

In contrast to the Late Oligocene/Early Miocene deformations D1 and D2, which affected the western and central part of the Salar de Antofalla area, the Mid-Miocene E–W to WNW–ESE shortening (D3) is confined to the eastern part only (Fig. 2). In the western part, no significant structural elements indicating compression younger than Early Miocene can be found.

Between the Salar de Antofalla and the Sierra de Calalaste (Fig. 2), tectonic activity produced a series of west-vergent reverse faults and thrusts trending parallel to the present Salar de Antofalla (Adelmann, 1997; Voss, in preparation). Early Paleozoic and Permian strata as well as older Tertiary sediments were affected. Uplift formed a new highland from which coarse-grained sediments (lower part of the Juncalito Formation) were syntectonically shed into the basin (Fig. 7). The onset of alluvial fan sedimentation is documented by an age of 11.2 ± 0.3 Ma (ID-48), suggesting that deformation D3 is roughly correlative with the Quechua event which is widely recognized in the Puna-Altiplano and the Eastern Cordillera (Coira et al., 1982).

3.4. Pliocene–Quaternary (4 Ma–present, interval D4)

During the final deformation interval D4, further E–W to WNW–ESE contraction was accommodated. Structures indicating compressive deformation are apparent east of the present Salar de Antofalla where Middle Miocene to Pliocene sediments were deformed. The tectonic style can be described as thin-skinned tectonism as indicated by almost subhorizontal west-vergent thrusts and overturned folds within the playa deposits of the Juncalito Formation. Early Paleozoic, Permian, and older Tertiary strata of the adjacent Sierra de Calalaste (Fig. 2) were reverse faulted onto these sediments. Presumably, older reverse faults, that were active during the deformation interval D3, were reactivated.

In the southern part, at the eastern border of the present Salar de Antofalla, the age of deformation D4 is indicated by undeformed ignimbrites [3.605 ± 0.005 Ma (ID-11)] unconformably overlying folded Juncalito sediments. Farther east, the same ignimbrite unit is intercalated in alluvial fan sediments of the Escondida Formation which were tilted synsedimentarily.
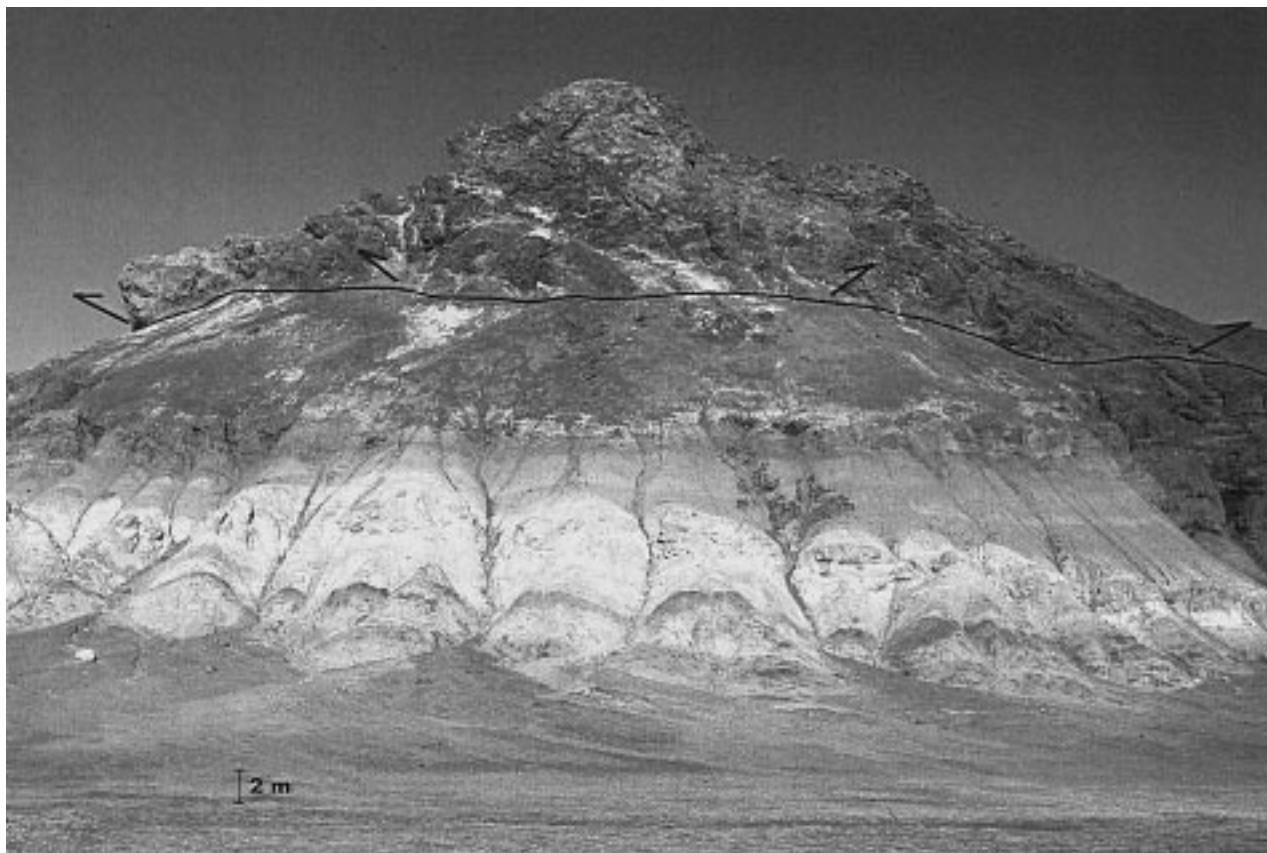
Fig. 8. Exposure located approx. 20 km south of the Vega Quiñoas showing thrusting of crystalline basement rocks (above) onto sediments of the Chacras Formation (below). View towards the east, exhibiting the N–S trending thrust. The thrust system which is exposed along the entire Salar de Antofalla was triggered due to the compressional deformation D1. Syntectonically, the Chacras Formation composed of proximal fan conglomerates was shed from the adjacent crystalline basement high.

Apparently, shortening can be correlated with the "Diaguita phase" described by Salfity et al. (1984).

Contraction was followed by strike-slip movements visible at the NE-trending right-lateral Acazoque strike-slip fault (e.g., Segerstrom and Turner, 1972; Marrett et al., 1994) crosscutting older D4 reverse faults and thrusts (Fig. 2). This significant structure exhibits right-lateral displacement and terminates in a "horsetail splay" or "extensional imbricate fan" respectively (sensu Christie-Blick and Biddle, 1985; Woodcock and Fischer, 1986) (Fig. 10). The Acazoque strike-slip fault system was active during Pliocene times. A basaltic andesite from the Acazoque valley (north of Cerro Beltrán) deformed by this fault system indicates that deformation is younger than 5.3 ± 0.3 Ma (ID-46). The change from contractional movements with WNW–ESE shortening to a strike-slip deformation with ENE–WSW shortening was also observed in surrounding parts of the Puna and the adjacent Eastern Cordillera by Marrett et al. (1994). They postulated the onset of the strike-slip movements at 2 Ma. Also, in the Salar de Incahuasi area, Late Pliocene sediments [1.7 ± 0.1 Ma (ID-73)] can be observed, which were affected by strike-slip move-ments. There, a reactivation of N to NNE-trending faults with a lateral component is presumed.

Additionally, at the southwestern border of the Salar de Antofalla, some slope-parallel normal faults occur (Fig. 2), interpreted as gravity slide effects due to the steep relief. Because of their limited distribution and displacement, they are not thought to be basin-forming.

4. Cenozoic volcanism: structures and age

In the Salar de Antofalla area, volcanic activity was significant during the Cenozoic but also occurred during the Permian and Early Jurassic, as indicated by some lavas and thin pyroclastic layers. Cenozoic volcanism is mainly documented by recently inactive stratovolcanoes and monogenetic vents. The products of these centers comprise pyroclastic rocks and lavas which occur as intercalations or at the top of the stratigraphic sequence. Important features include many low-volume ignimbrites (< 10 km^3) and few larger widespread ignimbrite sheets. New K–Ar and ^{40}Ar/^{39}Ar mineral and whole rock ages reflect volcanic

Fig. 9. Outcrop located 10 km southeast of the Volcán Antofalla showing west-vergent reverse faulting of phyllites of the crystalline basement (right) onto conglomerates of the Potrero Grande Formation (left). At the fault contact, the conglomerates display progressive angular unconformities indicating coeval alluvial fan sedimentation and Mid-Miocene compressive deformation D2. Intercalated in the conglomeratic succession, a tuff layer yielded an age 18.5 ± 0.5 Ma (ID-40).

activity in the Salar de Antofalla area or its vicinity at least from the Late Eocene to Late Pleistocene. The volcanic evolution during this time interval can be subdivided into three periods based on changes in the volume and composition of the volcanic products and on different structural features. Age data are given in Table 1.

4.1. Late Eocene–Early Miocene

The first stage, from Late Eocene to Early Miocene, is characterized by relatively low volcanic activity. Throughout the working area, only a few thin (<15 cm) pyroclastic layers intercalated within the sedimentary strata have been found. They are intermediate to acid crystal-rich ash-fall tuffs which consist of feldspar, brown hornblende, (oxy)-biotite, and quartz in a glassy to recrystallized, fine-grained matrix. Their scarce occurrence, fine-grained texture, and the lack of lithic components indicate that the eruptive centers of the pyroclastic rocks were located outside the study area, perhaps in the present Chilean

Precordillera. Their ages range from 37.6 ± 0.3 Ma (ID-64) to 22.5 ± 0.6 Ma (ID-18).

4.2. Early Miocene–Late Miocene

The second stage is marked by a dramatic increase in volcanic activity during the Middle Miocene, expressed by the development of several stratovolcanic centers. These centers (Cerro Beltrán, Cerro Tebenquicho, Volcán Archibarca, Fig. 2) are built up by voluminous long-lived compound flow and dome complexes. The Volcán Antofalla complex consists of a group of stratovolcanoes. They are mainly made up of silicic andesites, dacites, and rare rhyolites. Ignimbrites and pyroclastic fall deposits of the same age are widespread in the area. The ignimbrites have low volumes and are generally of the valley-fill type, with the exception of the plateau-forming Tambería ignimbrite (Fig. 2). Because of the numerous andesitic-dacitic stratovolcanoes, the assignment of individual ignimbritic units to specific eruptive centers is often unclear. The main outcrops are situated in the west
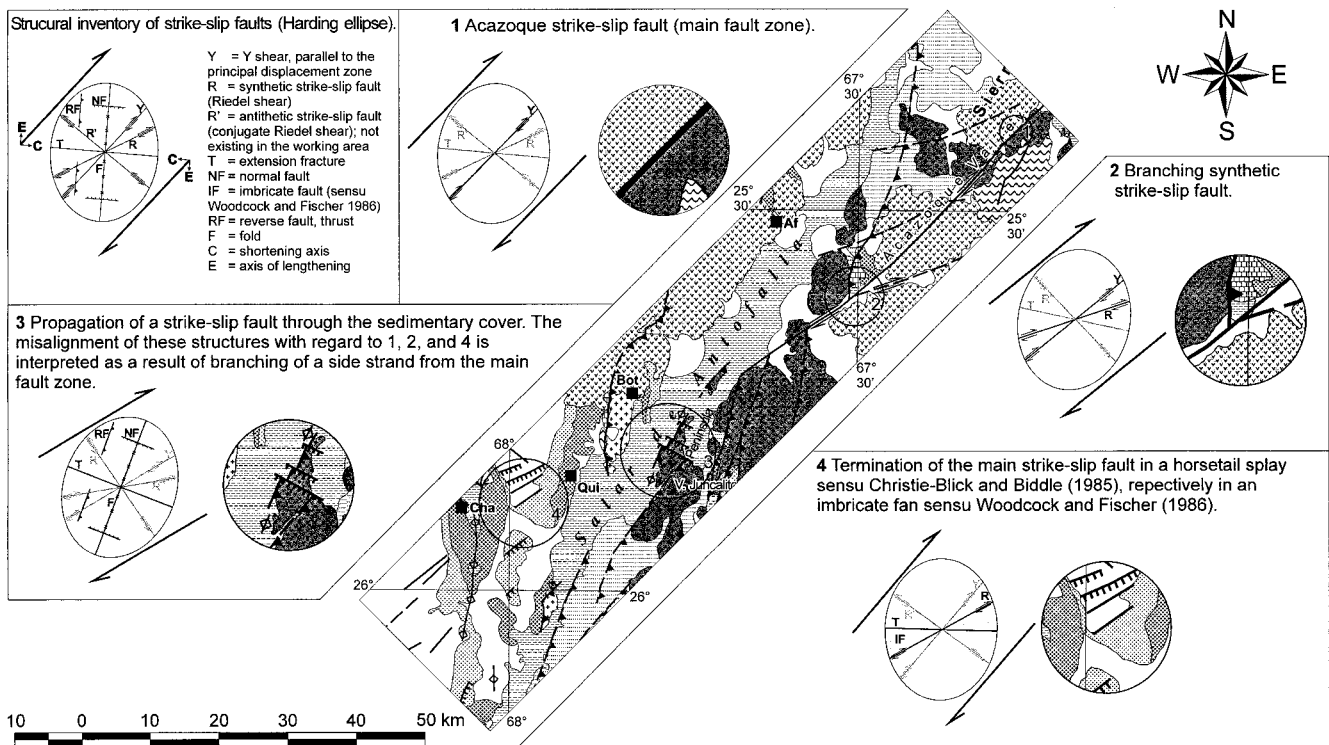
Fig. 10. Structural inventory of the right-lateral Acazoque strike-slip fault. For abbreviations and legend see Fig. 2.

and northwest of the Salar de Antofalla and in the south of the Salar de Incahuasi.

New radiometric ages (Table 1) allow a general survey of the eruptive history of stratovolcanic complexes and pyroclastic deposits. The earliest stratovolcanic eruptions are indicated by andesitic boulders in conglomerates of the Potrero Grande Formation. Intercalated volcaniclastic rocks and various pumice-fall tuffs yielded ages of 18.5 ± 0.5 Ma (ID-40) and 18.0 ± 0.6 Ma (ID-52). The oldest age for stratovolcanic lavas stems from a dacitic lava flow of Cerro Beltrán [14.1 ± 0.4 Ma (ID-36)]. Younger ages of several intermediate lava flows of the Cerro Beltrán and the Cerro Tebenquicho (ID-25, 26, 41) document the continuous build-up of stratovolcanic complexes up to the Late Miocene [5.96 ± 0.03 Ma (ID-27)]. The oldest ignimbritic rocks are exposed in the Agua Escondida Ignimbrite dated at 15.0 ± 1.0 Ma and 13.5 ± 1.5 Ma (Coira and Pezzutti, 1976; Coira et al., 1993). They are followed by some ignimbrites dated between 10.9 ± 0.3 Ma (ID-83, valley of Antofalla village) and 9.6 ± 0.2 Ma (ID-65, Potrero Grande). The youngest pyroclastic rocks of this stage occur south of the Salar de Incahuasi [6.3 ± 0.2 Ma (ID-72)].

The stratovolcanic complexes are located along the NW-trending Archibarca lineament which crosses the Western Cordillera (Salfity, 1985). Faulting of the centers related to the lineament has not been noted. The lineament has been interpreted as a zone of crustal weakness (Salfity, 1985).

4.3. Late Miocene–Pleistocene

The characteristic features of the third stage are numerous monogenetic centers and a widespread ignimbrite sheet. The eruptions of this type were accompanied by activity of the stratovolcanoes, as documented by intermediate lavas and low-volume ignimbrites [Ignimbrites: e.g., south of Salar Incahuasi, ignimbrite Campo de la Piedra Pómez, 0.2 ± 0.1 Ma (ID-71); lava flows dated by Coira and Pezzutti (1976): Cerro Cajeros basaltic andesite, 4.8 ± 2.5 Ma; Aguas Calientes basalt, 2 ± 1 Ma].

The monogenetic centers consist of cinder cones and lava flows characterized by low volume (< 2 km^3) of mainly basaltic andesites and subordinate basalts, andesites, and dacites. Based on their ages two groups can be defined. Most of our age data lie in the range between 5.3 ± 0.3 Ma and 3.61 ± 0.02 Ma (ID-46, 42, 30, 56, 17, 13), although two older ages of andesitic flows [12.8 ± 1.2 Ma (ID-20), 7.0 ± 0.3 Ma (ID-87)] have been obtained. The centers of this age range greatly dominate the monogenetic suite. These cones are partly eroded and their lava flows exhibit levelled surfaces. We suggest, therefore, that monogenetic activity reached a maximum at this time. The interval of maximum activity was followed by a more quiet period

which continues up to the present. There are a few younger cones which are almost perfectly cone-shaped with steep slopes and fresh rugged flow surfaces. One of these cones, at the southern edge of the Salar de Antofalla, has been dated at 0.2 ± 0.09 Ma (ID-9).

To the east of the Salar de Antofalla, the cinder cones are located at NE and N-trending reverse fault and thrust systems. We propose that magma ascent between 6 and 4 Ma was made possible by the relaxation between the deformation phases D3 and D4. In the northwestern part, structural control on cone formation is not obvious.

The second prominent feature of the youngest stage is the Vallecito ignimbrite sheet (10–100 km^3) which crops out south and southwest of the Salar de Antofalla. Its maximum thickness, measured at the western border of the Salar de Antofalla, is 20 m. In part the ignimbrite fills the southern section of the salar basin. Its source was presumably located west of the salar. Two pumice-poor flow units have been distinguished; the upper unit has an age of 3.605 ± 0.005 Ma (ID-11).

5. Petrography and geochemistry of the volcanic rocks

Petrographical and geochemical analyses have been carried out on the Miocene to Pleistocene volcanic rocks. Classification of these volcanites is taken from the SiO$_2$–K$_2$O diagram (Fig. 11) of Le Maitre (1989).

The Miocene lavas of the stratovolcanic complexes are high-Si andesites and dacites. Petrographically, they are similar and usually highly porphyritic. Almost aphyric rocks also occur and phenocryst contents vary, therefore, between 5–40 vol%. Plagioclase, (oxy)-hornblende, (oxy)-biotite, quartz, orthopyroxene, and Fe–Ti-oxides are the main phenocrysts. Minor constituents and accessory phases vary between centers and comprise olivine, clinopyroxene, apatite, zircon, and sphene. The matrix consists of lath-shaped plagioclase and glass devitrified to various extents. A detailed description is given in Kraemer (1999).

The ignimbrites are dacitic to rhyolitic in composition and range from non- and poorly-welded to strongly welded types. According to the degree of welding and the lithic content in the matrix, their color varies between light gray, gray, brown, reddish, and black. They differ greatly in grain size, type of lithic fragments, and amount of phenocrysts. The lithic components usually correspond to the local surface lithology. Phenocryst contents of matrix and pumice vary from 1 to 40 vol%. Plagioclase, quartz, and biotite occur as the main mineral phases in a glassy groundmass. Hornblende, orthopyroxene, clinopyroxene, Fe–Ti-oxides, and sanidine are confined to individual ignimbrite units.

The monogenetic basaltic to intermediate rocks exhibit a black, vitrophyric texture and range from nearly aphyric to porphyritic (2–20 vol% phenocrysts). Andesitic rocks display the highest phenocryst content. Among the basaltic and basaltic andesitic rocks, olivine and clinopyroxene (< 1 mm) predominate the phenocrystic assemblage. There are minor amounts of hornblende, Fe–Ti-oxides, and plagioclase. The groundmass is usually vitric with abundant plagioclase laths, olivine, and clinopyroxene. In the andesites, plagioclase, orthopyroxene, and hornblende prevail over clinopyroxene, olivine, and Fe–Ti-oxides. The groundmass mainly contains glass and lath-shaped plagioclase, as well as minor amounts of orthopyroxene, Fe–Ti oxides, and hornblende. Large feldspar and quartz xenocrysts (up to 2 cm) rimmed by clinopyroxene, occur and have been described by various authors (Pichler and Zeil, 1972; Schreiber and Schwab, 1991; Kay et al., 1994a) as important features of Pliocene and younger monogenetic lavas of the Puna.

Geochemically, the volcanic rocks of the Salar de Antofalla region follow the calcalkaline trend and belong to the medium-K to high-K-suite. (Table 2, Fig. 11). The shift from intermediate to more basic magmatic composition with time, as noted earlier by Coira and Pezzutti (1976), can be shown clearly. Whereas Miocene lavas from stratovolcanoes have andesitic to dacitic composition, the Late Miocene to Pleistocene monogenetic lavas show mostly basaltic andesitic composition.

The Miocene stratovolcanic andesites and dacites of the Salar de Antofalla area derived from subduction-related mantle sources with arc character as displayed by elevated Ba/La, La/Ta, and Ba/Ta ratios (Figs. 12 and 13). The lower backarc values (e.g., Ba/La 17 - 20) of some Tebenquicho lavas can be interpreted as being consistent with the position of the centers in the back of the volcanic front. Kay et al. (1994a) attributed lower Ba/La ratios to the depletion of Ba from the subduction component by arc magmas along the frontal volcanic line.

In terms of crustal evolution, most interesting are the intermediate lavas of the Cerro Beltrán [14.1 Ma–7.7 Ma (ID-36, ID-41)] and the Cerro Tebenquicho [11.0 Ma–5.96 Ma (ID-26, ID-27)]. They are characterized by high contents of incompatible elements (K$_2$O, Th, Pb, Rb, Table 2, Fig. 11) and show high Sr isotopic ratios and low Nd isotopic ratios (Fig. 14). Concerning restitic olivine in some Tebenquicho lavas, both observations are interpreted as contamination of intruding basaltic magmas within the Andean continental crust. This is consistent with the higher Sr isotopic ratios and lower Nd isotopic ratios of the nearby Cerro Galán caldera ignimbrites which have been interpreted to be of crustal origin (Francis et al., 1989).
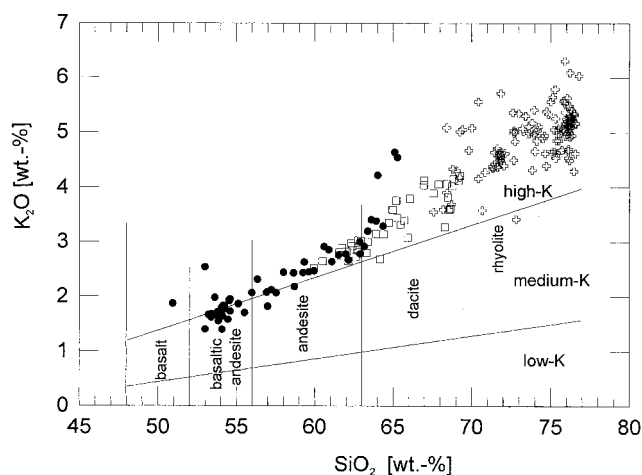
Fig. 11. SiO$_2$–K$_2$O diagram of volcanites from the Salar de Antofalla area. Black dots (●) represent monogenetic cones (<7 Ma), open squares (□) the stratovolcanoes (approx. 6–14 Ma) and crosses (✧) the ignimbrites (10.9–0.2 Ma).

Fig. 12. SiO$_2$–Ba/La diagram of monogenetic cones (black dots ●) and stratovolcanoes Cerro Tebenquicho (open triangles △) and Cerro Beltrán (open squares □). Arc and backarc ranges after Mpodozis et al. (1995).

Cerro Beltrán lavas and some intermediate samples of Cerro Tebenquicho show strongly fractionated La/Yb ratios (37–47, Fig. 15) controlled by low contents of the heavy rare earth elements (HREE). As garnet accommodates preferentially the HREE, high La/Yb ratios point to high pressure garnetiferous source rocks and have been frequently used to reconstruct Andean crustal thickening through time (Mpodozis et al., 1995; Kay et al., 1991; Coira et al., 1993). Together with moderate Na$_2$O and Sr contents (3.5–4.3 wt% Na$_2$O, 530 ppm Sr at 63 wt% SiO$_2$) and moderately negative Eu-anomalies (Eu/Eu* 0.74–0.86) we presume garnetiferous but also plagioclase-containing rocks of intermediate chemistry in the crustal source area of Beltrán and Tebenquicho lavas. However, the minimum pressure at which garnet appears in the residual mineralogy in perceivable amounts is questionable. Experimental results on basaltic compositions argue for a garnet-in reaction between 10–12 kbar (Green, 1982; Rapp et al., 1991; Wolf and Wyllie, 1994). Fractionated REE patterns like in the Beltrán lavas were found at pressures of 16 kbar (Rapp et al., 1991). Therefore, the chemistry of the Beltrán and Tebenquicho lavas indicates that the Middle Miocene crustal thickness was at least 33–40 km. Concerning tectonic shortening during the Late Oligocene (D1) and the Early Miocene (D2), the crust may have reached a thickness of at least 40 km during the Middle Miocene.

The geochemistry of the young monogenetic basaltic-andesitic rocks of the Puna has been described by Kay et al. (1994a). Although these rocks have incorporated crustal components during their ascent through the thickened continental crust, they are still primitive enough to display their mantle source.
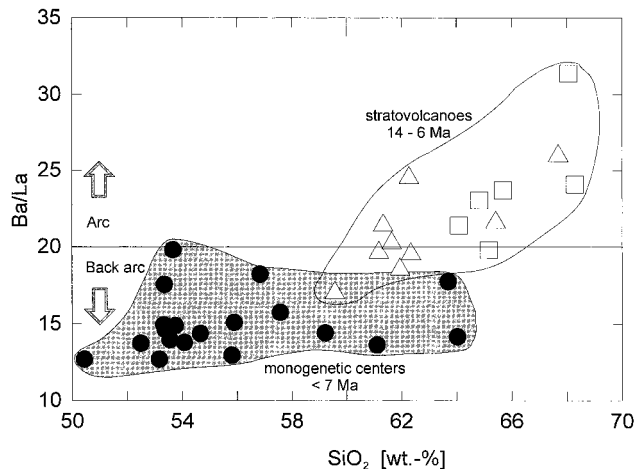
Beneath the Salar de Antofalla area low La/Ta ratios (<25, Fig. 13) of some flows indicate an intraplate-like mantle source. Compared with shoshonitic rocks of the Central Puna, the Antofalla rocks point to a higher percentage of mantle melting (Kay et al., 1994a). Low Ba/La ratios (<20, Fig. 12) of the Puna monogenetic rocks are consistent with their position in the back of the volcanic front.

6. Evolutionary model

Data for the sedimentary facies, deformation, and volcanism of the Salar de Antofalla area are integrated to put forward a model for the Cenozoic evolution of the Southern Puna (Fig. 16).

Before the beginning of crustal thickening and uplift of the Central Andes during Neogene times, the Salar de Antofalla area was part of the Andean foreland. Apatite fission track data on a Paleozoic granite intruded in Precambrian metamorphic basement reveal cooling to near surface temperatures between 80–40 Ma ago (analysis carried out by Donelick Analytical Inc.). The granite is exposed at the western border of the present Salar de Antofalla south of Quiñoas. We conclude, therefore, that Precambrian rocks were probably exposed at least during the Paleogene in the Southern Puna. The Southern Puna may have been part of a large region with low relief in which only minor sedimentation occurred up to the Late Eocene.

Later on, the Salar de Antofalla area was incorporated into the Andean orogen. Sedimentological and tectonical features as well as geochemical data for the volcanic rocks show that the area transferred from a foreland to an intra-arc setting. Finally, it is situated behind the active volcanic front and shows geochem-

Table 2
Representative geochemical analyses of volcanites from the monogenetic centers, stratovolcanoes, and pumices of ignimbrite units from the Salar de Antofalla area (Ant. d.l. Sa.: Antofagasta de la Sierra, Qda. Archib.: Quebrada Archibarca, C.P. Pómez: Campo de la Piedra Pómez, Potr. Gde: Potrero Grande, for location see Fig. 2)

Locality	Monogenetic vents (~6.0–3.6 Ma)					Stratovolcanoes (~14.0–6.0 Ma)						Ignimbrites (<11.0 Ma)		
	Peninsula region				Ant. d.l. Sa.	Beltrán			Tebenquicho			Qda. Archib.	C.P. Pómez	Potr. Gde.
Sample	An-16	An-23	An-42	An-44	An-187	An-184	An-185 (ID-41)	An-188 (ID-36)	An-125	An-136 (ID-26)	An-182 (ID-27)	SIA-32b1	SIA-97b1	SIA-68b2b
Age [Ma]							7.7 ± 0.2	14.1 ± 0.4		11.0 ± 0.5	5.96 ± 0.03			
[%]														
SiO_2	60.00	62.8	52.00	49.7	53.77	67.66	64.64	63.99	65.31	60.54	59.67	72.68	71.48	71.79
TiO_2	1.336	0.896	1.437	1.551	1.28	0.504	0.794	0.868	0.71	1.003	1.128	0.1	0.24	0.11
Al_2O_3	15.5	15.9	15.5	14.8	16.06	15.59	15.6	15.9	15.74	15.74	15.9	13.16	13.62	12.29
Fe_2O_3	6.42	4.96	8.25	9.23	8.79	3.36	4.44	4.86	4.35	6.24	6.62	0.73	1.45	0.71
MnO	0.08	0.063	0.127	0.154	0.13	0.045	0.053	0.061	0.062	0.094	0.084	0.09	0.06	0.08
MgO	3.21	2.14	7.68	8.66	7.41	1.31	2.18	2.47	1.9	3.31	4.13	0.18	0.37	0.15
CaO	5.25	4.41	7.61	9.16	7.71	3.4	4.08	4.32	4.29	5.35	5.77	0.68	1.32	1.5
Na_2O	3.35	3.46	2.92	2.99	3	4.17	3.9	4.02	3.88	3.64	4.08	3.01	3.75	2.86
K_2O	2.69	3.21	1.92	1.83	1.82	3.24	3.27	3.12	3.37	2.76	2.5	4.88	4.84	4.91
P_2O_5	0.36	0.24	0.38	0.452	0.217	0.133	0.223	0.246	0.213	0.296	0.309	0.05	0.08	0.02
H_2O	0.27	0.28	0.33	0.19	0.58	0.61	1.65	0.3	0.48	1.31	0.29	3.88	2.03	2.93
CO_2	0.11	0.07	0.09	0.14	0.15	0.14	0.07	0.08	0.12	0.08	0.08	0.06	0.11	2.27
Σ	98.58	98.43	98.25	98.86	100.93	100.16	100.90	100.24	100.43	100.36	100.56	99.50	99.35	99.62
[ppm]														
Cr	77	38	310	378	329	33	56	64	41	107	177	< 10	< 10	< 10
V	148	108	177	250	209	70	105	112	94	128	152	< 10	16	< 10
Ni	114	16	156	122	177	< 10	18	24	14	33	52	< 10	< 10	< 10
Zn	103	84	93	86	87	62	81	87	73	85	96	40	37	32
Rb	83	124	49	39	48	150	132	113	116	77	78	131	173	220
Sr	591	497	642	911	383	340	421	525	503	533	607	108	241	62
Y	19.28	11	20.97	25.22	23.86	10.17	13.47	12.47	12.16	19.3	15.29	15	19	18
Zr	255	212	197	185	135	142	183	236	196	217	233	70	171	80
Nb	18.1	–	36.08	30.59	16.7	7.39	11.73	11.24	13.07	19.52	14.34	–	–	–
Cs	1.18	–	1.38	1.1	1.69	5.76	5.39	2.02	4.02	2.5	2	–	–	–
Ba	632	709	469	609	390	737	655	798	744	717	664	1063	639	609

Table 2 (continued)

| Locality	Monogenetic vents (~6.0–3.6 Ma)				Ant. d.l. Sa.		Beltrán	Stratovolcanoes (~14.0–6.0 Ma)		Tebenquicho		Qda. Archib.	C.P. Pómez	Ignimbrites (<11.0 Ma) Potr. Gde.
	Peninsula region													
Sample	An-16	An-23	An-42	An-44	An-187	An-184	An-185 (ID-41)	An-188 (ID-36)	An-125	An-136 (ID-26)	An-182 (ID-27)	SIA-32b1	SIA-97b1	SIA-68b2b
Sc	10.7	8.5	20.5	27	24.3	5.6	7.4	8	5.8	10.4	12.8	2.2	3.1	2.9
La	50	50	39	49	19.69	23.5	33.12	37.29	34.47	36.57	39.07	17	26	27
Ce	107	96	78	85	43.1	47.19	75.91	86.79	74.9	74.12	84.32	31	47	43
Pr	12	10	8.7	11	5.5	5.36	8.05	9.06	8.09	9.09	10.25	4.1	5.7	5.8
N	46	38	33	44	21.65	18.22	30.21	33.01	28.09	33.25	38.19	13	19	19
Sm	8.7	6.6	6.4	7.9	4.7	3.5	5.31	5.71	5.06	6.04	6.67	2.9	3.7	3.5
Eu	1.9	1.4	1.7	2.1	1.24	0.8	1.22	1.32	1.28	1.56	1.65	0.56	0.45	0.47
Gd	6.4	4.5	5.4	5.9	3.58	3.33	4.34	4.5	4.25	5.21	5.3	2.6	3.2	3
Tb	0.82	–	0.8	0.88	0.54	–	0.47	0.5	–	0.59	0.55	0.45	0.51	0.49
Dy	4	2.5	4.2	4.5	3.62	1.86	2.26	2.31	2.29	3.27	2.82	2.7	3.3	3.2
Ho	0.67	0.39	0.74	0.84	0.63	–	0.39	0.37	–	0.58	0.46	0.52	0.66	0.58
Er	1.7	1	2.1	2.3	1.95	0.88	0.98	0.98	1.05	1.52	1.2	1.6	2	1.9
Tm	0.23	0.16	0.29	0.32	0.25	–	0.13	0.13	–	0.2	0.14	0.25	0.3	0.3
Yb	1.3	0.7	1.8	2	1.88	0.76	0.82	0.79	0.9	1.33	0.96	1.6	2.1	2
Lu	0.2	0.12	0.26	0.3	0.26	–	0.12	0.11	–	0.16	0.14	0.25	0.33	0.3
Hf	6.37	–	3.81	4.06	3.47	3.84	4.03	5.6	3.95	4.08	5.43	–	–	–
Ta	1.25	–	2.66	2.01	–	0.63	0.92	0.81	1.11	1.58	1.54	–	–	–
Pb	10.89	–	6.45	6.38	7.54	21.35	15.14	13.58	13.68	11.15	10.71	–	–	–
Th	11.15	–	7.48	8.29	5.3	11.63	16.2	14.12	13.66	11.97	11.18	–	–	–
U	1.46	–	1.29	1.34	1.34	3.18	3.38	1.76	2.83	1.99	1.97	–	–	–
$m^{87}Sr/^{86}Sr$	0.708944	–	0.705727	0.705050	–	–	0.709052	0.708716	–	0.708525	0.708023	–	–	–
$d(m^{87}Sr/^{86}Sr)$	0.000023	–	0.000018	0.000018	–	–	0.000012	0.000008	–	0.000009	0.000014	–	–	–
$\delta^{18}O[‰]$	7.25	–	7.86	7.39	–	–	–	7.92	–	–	–	–	–	–
$m^{143}Nd/^{144}Nd$	–	–	–	0.512613	–	–	0.512314	0.512330	–	0.512375	0.512369	–	–	–
$(m^{143}Nd/^{144}Nd)$	–	–	–	0.000005	–	–	0.000006	0.000006	–	0.000005	0.000009	–	–	–
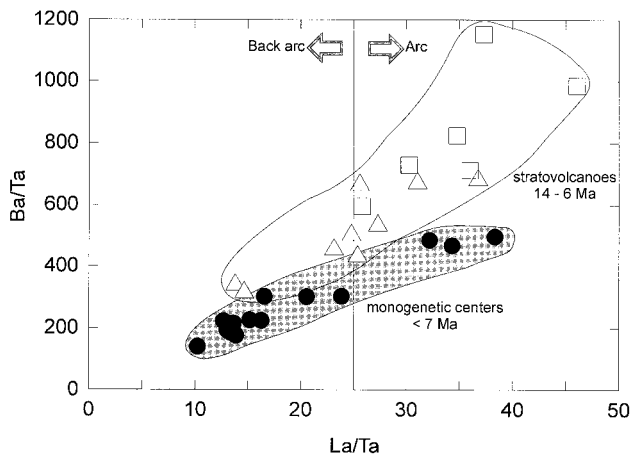
Fig. 13. La/Ta–Ba/Ta diagram of monogenetic cones and stratovolcanoes Cerro Tebenquicho and Cerro Beltrán. Symbols as in Fig. 12. Arc and backarc ranges after Mpodozis et al. (1995).

Fig. 15. SiO$_2$–La/Yb diagram of monogenetic cones and the stratovolcanoes Cerro Tebenquicho and Cerro Beltrán. Symbols as in Fig. 12.

ical features of a backarc position, but also tectonic and sedimentological attributes of an intra-arc setting. This evolution is described stepwise following the sequence of tectonic, volcanic, and sedimentary events.

6.1. Late Eocene to Late Oligocene (38–28 Ma)

During latest Eocene to Late Oligocene, relatively uniform nonmarine clastic sediments (Quiñoas Formation) were deposited across the entire Salar de Antofalla area (Adelmann, in preparation) which represented, consequently, a coherent sedimentation area. It was presumably part of larger retroarc foreland basin whose detritus derived from the Incaic mountain belt in the west (Jordan and Alonso, 1987). This oro-

Fig. 14. Sr and Nd initial isotopic compositions of intermediate stratovolcanic lavas and a basaltic monogenetic center of the Salar de Antofalla area. Due to the uncertain age, the isotopic ratios of the basaltic flow have not been corrected. The originating error is negligible because of the young age (<7 Ma) of the sample. Symbols as in Fig. 12. For comparison note the data for the Galán Ignimbrite from Francis et al. (1989), mantle array after Hawkesworth (1979), and CVZ array after Davidson et al. (1991).
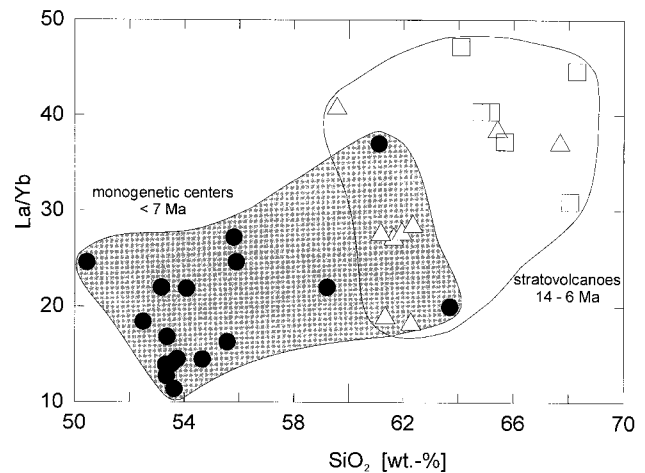
genic belt, today represented by the Chilean Precordillera, developed during the Incaic deformation phase (approx. 38 Ma, Döbel et al., 1992) and was the site of the Late Cretaceous–Paleogene Andean magmatic arc. Due to the small amount of shortening in the Incaic mountain belt (~20%) and the tectonic style (Günther et al., 1998), thrust loading may not have been the main subsidence mechanism. Subsidence presumably resulted from sedimentary loading or, as proposed by Jordan and Alonso (1987), from thermal contraction due to cooling of the Late Cretaceous–Paleogene arc.

Distant magmatic activity is indicated by a few pyroclastic fall deposits. Probable sources of the pyroclastic rocks are in the Franja de Maricunga (26°S–28°15′S, adjacent to the west of the present Western Cordillera) where intermediate volcanic and plutonic rocks of equivalent age are exposed. They represent the final products of the magmatic arc (Kay et al., 1994b; Mpodozis et al., 1995; 36–30 Ma). Consequently, the Southern Puna was located east of the magmatic arc of the Early Tertiary subduction system, in the foreland. Following Pilger (1984), a flat subduction angle during this time can be assumed which would have been caused by subduction of progressively younger and, therefore, hotter oceanic crust of lower density.

6.2. Late Oligocene–Early Miocene (28–20 Ma)

A change in basin geometry occurred during the Late Oligocene when large amounts of coarse clastics (Chacras Formation) were deposited. As a consequence of west-vergent reverse faulting, basement rocks were uplifted and eroded along the entire recent Salar de Antofalla. This intrabasinal Antofalla high
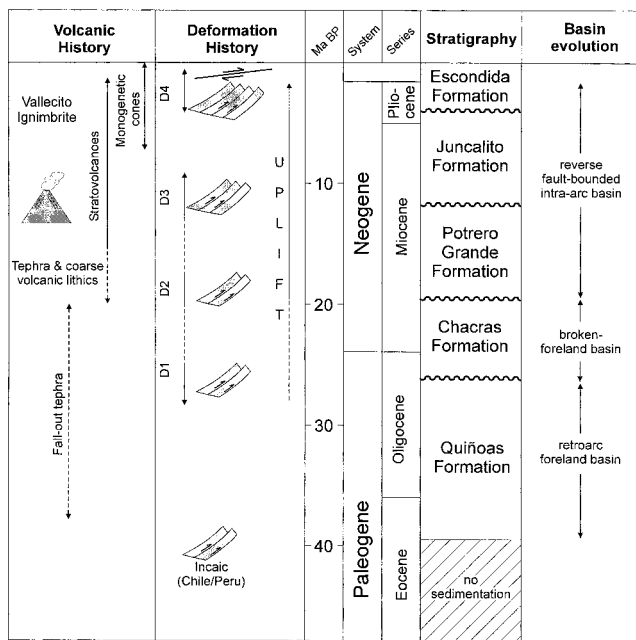
Fig. 16. Evolutionary model for the Salar de Antofalla area illustrating the magmatic and structural development as well as the stratigraphy and basin history.

(Voss, in preparation) extends over about 120 km which is indicated by petrographical and paleocurrent data (Fig. 7) as well as by the facies distribution of the Chacras sediments (Adelmann, in preparation). Due to the basement-involved contractional tectonism, the former coherent part of the foreland basin was segmented into smaller broken-foreland basins (Adelmann and Görler, 1998). Tectonic shortening (D1) could have caused initial crustal thickening and uplift of the Southern Puna.

Distal magmatism is documented by a few pyroclastic layers. After a pause during the Late Oligocene, volcanic activity was renewed in and south of the Franja de Maricunga (26–21 Ma, Mpodozis et al., 1995) and was initiated in the Western Cordillera immediately adjacent to the Salar de Antofalla area (<23 Ma, Naranjo and Cornejo, 1992). The Southern Puna still remained east of the magmatic arc.

The renewed magmatism of the Franja de Maricunga, the beginning of volcanism farther east in the Western Cordillera, and the development of a broken-foreland basin occurred contemporaneously with an increase in convergence rate (28.3–25.8 Ma, Somoza, 1998) normal to the trench due to reorganization of the Pacific plate's motion (Pilger, 1984; Pardo-Casas and Molnar, 1987). Kay et al. (1988, 1991) and Mpodozis et al. (1995) inferred a subduction angle of <30° at this time.

6.3. Early Miocene–Middle Miocene (20–12 Ma)

This time interval was characterized by prevailing regional compression and the onset of volcanic activity in the Salar de Antofalla area. The volcanic arc broadened from the present Western Cordillera to the Antofalla area. The geochemical data of the volcanic rocks of the Antofalla area predominantly display an arc signature. Ongoing thick-skinned compressive deformation caused a further segmentation into basins bounded by east-vergent reverse faults in the west and west-vergent reverse faults in the east. Due to their incorporation into the magmatic arc, they are classified as fault-bounded intra-arc basins. Syntectonic sedimentation was related to the activity of fault systems indicated by progressive angular unconformities. The sedimentation also was largely influenced by the spatial distribution of the vigorously forming stratovolcanoes. As a result, the distribution of highlands and accumulation areas is obscure.

According to geochemical data, the volcanic melts erupted through a crust whose thickness measured at least 40 km. This coincided with contractional tectonism and suggests that regional uplift was in progress.

6.4. Middle Miocene–Early Pliocene (12–4 Ma)

During Middle Miocene times, a peak of tectonic activity changed the basin configuration. Several reverse fault-bounded intra-arc basins were developed due to tectonic shortening at about 12–10 Ma. Syntectonically, large amounts of alluvial fan sediments were deposited. The Salar de Antofalla basin itself presumably extended to the area between the western margin of the recent Salar de Antofalla and the Sierra de Calalaste (Adelmann, 1997; Voss, in preparation). Sedimentation patterns were mainly controlled by the position of reverse faults and thrusts at its eastern margin. Therefore, features of this highly elongated basin are an asymmetric shape in cross section as well as a wedge-shaped and unidirectional facies distribution (Adelmann, 1997).

Volcanic activity of the stratovolcanic centers continued. A position behind the volcanic front, but within the volcanic arc is indicated by geochemical data of the volcanites. Ongoing magmatism and contractional tectonism may have caused further crustal thickening and uplift.

Because arc volcanism in the Southern Puna continued, a relatively flat subduction angle could be assumed. This slab angle and the onset of contractional tectonism could have been provoked by the interaction of the San Juan Fernández ridge with the South American Plate. According to Pilger (1984), the subduction of this aseismic ridge is inferred to have caused the segment of present flat slab subduction in

Central Chile (28–33°S). Due to its NE-strike, the ridge came into contact with the South American plate first in N Chile and then migrated southwards along the trench to its present position in Central Chile. According to von Huene et al. (1997), the San Juan Fernandez ridge passed the entire segment of flat subduction (28°–33°S) south of the Salar de Antofalla during the past 8 my. Assuming the same migration velocity, subduction of the ridge could have begun at the latitude of the Salar de Antofalla 2–3 my earlier, consequently at about 11 Ma.

During Late Miocene to Pliocene times (< 9 Ma), alluvial fan sedimentation was interrupted by a period of relative tectonic quiescence. Due to the decreased clastic input, this period is marked by the abundance of lacustrine carbonates and sulfates deposited in marginal parts of the basin. Abundance of halite and sulfate evaporation in the central part of the basin may indicate the establishment of an internal drainage at about 8–9 Ma.

Between 6 and 4 Ma, the relative tectonic quiescence was accompanied by the eruption of a major volume of intraplate-like basaltic andesitic magmas at monogenetic centers. As pointed out by Kay et al. (1997), eruption of these centers was contemporaneous with eastward migration (∼50 km) of the volcanic front due to an overall shallowing of the subducting slab. The geochemical data of the basaltic andesites are consistent with their position in the back of the volcanic front.

Kay et al. (1994a) showed that the occurrence of intraplate-like volcanism is associated with crustal heating, a generally higher topography, and a thinner lithosphere of the Southern Puna compared with the Altiplano. They interpreted these features as a consequence of lithospheric delamination. Our age data suggest that if delamination had indeed occurred this process could have been of major importance between 6 and 4 Ma.

6.5. Early Pliocene (4 Ma–present)

During this stage further crustal thickening and uplift resulted from renewed contractional movements (< 4 Ma). Shortening is indicated by reverse faulting and thrusting at the eastern edge of the Salar de Antofalla (Voss, in preparation) reducing the basin to its actual narrow and elongated shape. This relief-forming tectonism caused shedding of large amounts of alluvial fan deposits (Escondida Formation). Basin-forming tectonic processes and distribution of large stratovolcanic centers which were mostly extinguished during the Pleistocene are comparable to the former stage. Therefore, the basins of the Southern Puna are further characterized by an intra-arc setting.

Revived tectonism was accompanied by decreasing

activity of monogenetic centers (geochemically representing backarc magmas) and stratovolcanoes as well as the eruption of the widespread Vallecito ignimbrite (3.6 Ma). According to De Silva (1989), large-volume ignimbrites, like the Vallecito ignimbrite, may be interpreted as reflecting large-scale crustal melting due to crustal thickening and heating by basaltic intrusions.

Today, the Southern Puna experiences a tectonically more quiet period indicated by very low seismic activity and by young alluvial fans that are usually undeformed.

7. Conclusions

1. Our model of basin evolution of the Salar de Antofalla area further develops previous models presented by Jordan and Alonso (1987), Alonso et al. (1991), and Vandervoort et al. (1995). Sedimentation started during the Late Eocene in an uniform basin which was part of a retroarc foreland basin related to the Incaic mountain belt, the present Chilean Precordillera. Further basin development is characterized by the segmentation of the uniform basin into several broken-foreland depocenters, followed by subdivision into fault-bounded intra-arc basins. Spatially discontinuous sedimentation resulted in variable thicknesses of Miocene–Pliocene strata which generally confirms observations in other parts of the Southern Puna (Alonso, et al., 1991; Vandervoort et al. 1995).

2. The tectonic regime of the Southern Puna has been dominantly compressive from the Late Oligocene to recent time, but the thick-skinned tectonism resulted only in minor amounts of shortening. Four compressive phases can be distinguished. Following Allmendinger et al. (1997), the major basin-forming mechanism during this time is block rotation in footwalls of range-bounded reverse faults. We did not find indications for lithospheric extension during the Early Miocene as suggested for the southern part of the Altiplano by Hérail et al. (1993) and Soler and Jiménez (1993).

3. Abundant stratovolcanic lavas and gravel of intermediate volcanic rocks of the Salar de Antofalla area point to an initiation of volcanism in the Southern Puna between 14 Ma and about 18 Ma. This coincides with the age of the oldest ash flow tuffs (< 17.2 Ma) in the root zones of long-lived volcanic centers of the central part of the Puna (Coira et al., 1993 and references therein). It precedes, however, the magmatic activity of the northern Puna where small stocks and domes developed < 13 Ma, but major stratovolcanoes and calderas did not form before 10 Ma (Coira et al., 1993).

Thus, during the Early to Middle Miocene, the continental crust of the Southern Puna may have received higher amounts of magmatic addition than the Northern Puna. If magmatic addition leads to thermal weakening of the lower portion of the crust, this pattern may have provoked different timing of tectonic shortening and crustal thickening in both parts of the Puna.

4. The timing of crustal thickening and uplift of the Puna plateau has been addressed by several authors (Allmendinger et al., 1997; Allmendinger and Gubbels, 1996; Whitman et al., 1996; Vandervoort et al., 1995; Kay et al., 1994a; Isacks, 1988). Whereas the major part of crustal thickening is attributed to shortening (Allmendinger et al., 1997; Isacks, 1988) which can be observed in the field, the reconstruction of uplift is based on indirect evidence. Besides fission track data (Masek et al., 1994; Benjamin et al., 1987; Crough, 1983) that yield information upon the time of exhumation, which in an arid climate may be delayed in respect to uplift, two approaches have been undertaken. One attempt has been made by Vandervoort et al. (1995) who suggested that the internal drainage of the Puna was established contemporaneously with uplift. As indication for the internal drainage, they took sedimentation of thick evaporites and interpreted that the uplift began between 14.1 and 24.2 Ma. Following this idea, our age data on thick halite deposits would argue for the beginning of uplift during the Middle Miocene at about 11 Ma. The second approach assumes that surface elevation is related to crustal thickness, which in turn increases by shortening and to a minor degree, by magmatic addition (Allmendinger et al., 1997; Isacks, 1988). Following this idea, uplift would have been started during the Late Oligocene deformation phase D1 (25–28 Ma).

The beginning of volcanism in the Salar de Antofalla area between 18 Ma and 14 Ma would mark an important increase in crustal thickness and uplift. As suggested by Allmendinger et al. (1997), thermal softening and thinning of the lithosphere by intruding magmas is a key condition for plateau development. A minimum crustal thickness of 40 km is evidenced by the comparison of geochemical data for Middle/Late Miocene (14–7 Ma) volcanic rocks with experimental data. Comparing geochemical data of volcanic rocks of the Western Cordillera (27°S, 30°S) southwest of the study area with modern analogues of the Andean Southern Volcanic Zone, Kay et al. (1991, 1994b) estimated a crustal thickness of 45 km during the Early Miocene and of 50–55 km during the Middle Miocene.

Taking into account our tectonic, geochemical, and sedimentological data, we believe that uplift and crustal thickening initiated during the Late Oligocene and continued with several pulses up to the present.

Appendix A

A1. Analytical methods

A1.1. Whole rock geochemistry

Rock samples of 3–5 kg were crushed and split, then ground in an agate mill to a grain size of $< 62 \mu m$. Sample homogeneity was assured by sieving, regrinding of oversize and homogenization.

Major and trace elements (Cr, Ni, V, Ba, Sr, Rb, Zn, Zr) were measured using X-ray fluorescence on fused discs. The analyses were made with an automated spectrometer of the type Siemens SRS303AS using a Rh tube operated at 50 kV and 45 mA. Accuracy and precision were improved by use of up to 40 reference rocks. Volatile components H_2O^+ and CO_2 were analyzed by infrared spectrometry (Leco RC-412) at 1100°C in an oxygen stream. Other trace elements were determined using the ICP-AES method (REE and Sc of samples An-16, An-23, An-42, An-44, SIA-32b1, SIA-97b1, SIA-68b2b) or the ICP-MS method (REE and remaining elements of the remaining samples). Sample dissolution for ICP-AES analyses were made following the method of Zuleger and Erzinger (1988). A Varian Liberty 200 spectrometer was used. Analytical precision has been improved to

be better than 10% for all elements except Tb (11%) using repeated analyses of within-run standard (JA-2, andesite). Sample dissolution for ICP-MS-analyses was achieved in pressurized teflon vessels with hot HF-HClO$_3$ for 17 h. Analyses were made with an VG Plasmaquad 2. Comparison with Zr concentration determined by XRF showed good agreement. The intensity was monitored with three internal standards (Re, Rh, In) and calibration was made with three standard solutions. Analytical precision was improved with in-house-standard BB (basalt) showing to be better than 10% for all elements except Ce and Yb (12%), as well as Tb, Er, Hf, and Sc (20%).

Isotopic compositions of Sr and Nd were measured with spectrometers of the type VG Sector 54-30 using Ta filaments (Sr) and Finnigan MAT 262 (Nd) using Ta filaments for evaporation and Re filaments for ionization. Samples were dissolved in pressurized teflon vessels for three days in 5:1 HF-HNO$_3$, then dried and taken up in HCl for chemical separation. Cation exchange resin (Biorad AG50W × 12) in quartz glass columns was used to separate the Sr fraction and the REE fraction. Nd was separated from the remaining REE in quartz glass columns with teflon (PTFE) powder coated with HDEHP (Bi-2ethyl-hexyl-phosphoric acid). Correction of mass fractionation was made using ^{88}Sr/^{86}Sr ratios = 8.3752 and ^{146}Nd/^{144}Nd ratio = 0.7219. The average value of NBS 987 Sr standard obtained during the measuring campaign was 0.710246 ± 5. Repeated analyses of the La Jolla Nd-standard gave an average value of 0.511855 ± 4.

Isotopic analyses of oxygen were done using a Finnigan MAT 251spectrometer. Sample preparation followed the method of Clayton and Mayeda (1963) using Ni-vessels and ClF$_3$ at 600°C. Analytical precision was improved with an in-house quartz standard and found to be better than 0.3‰.

A1.2. Age determination

K–Ar determinations were performed by Geochron Laboratories, Krueger Enterprises Inc. in Cambridge, Massachusetts, USA.

For the purpose of laser ^{40}Ar/^{39}Ar dating done at GEOMAR Forschungszentrum in Kiel, Germany, sanidine, plagioclase and biotite crystals were hand-picked from crushed pumice lapilli, lava fragments, and whole rock ignimbrite and fallout ash samples (ID-8, 11, 33, 48, 63, 64, 91, 94), and adhering glass or matrix removed in a diluted hydrofluoric acid bath (feldspars only). Whole rock and glass chips were washed in distilled water. All samples were subsequently cleaned with an ultrasonic disintegrator.

Samples were irradiated in 3 batches in the 5 MW reactor at the GKSS Research Center (Geesthacht) with a 1 mm cadmium foil shielding. During the irradiations, samples, monitors, calcium and potassium salts were kept in wells drilled into single aluminium disks. Stacks of 7–9 disks were held in tightly fitting cold-sealed Al capsules, and rotated during the entire irradiation (72–144 h), with the stack axis (rotational axis) vertical with respect to reactor coordinates. Taylor Creek rhyolite sanidine (TCR 85G003) was used as irradiation monitor, whose age has been determined at 27.92 Ma (Duffield and Dalrymple, 1990) relative to USGS primary standard SB-3 at 162.9 Ma (Lanphere et al., 1990). Corrections for interfering neutron reactions are based on the average ^{36}Ar/^{39}Ar$_{Ca}$-, ^{37}Ar/^{39}Ar$_{Ca}$-, and ^{40}Ar/^{39}Ar$_K$-ratios measured on optical grade CaF$_2$ and high purity K$_2$SO$_4$ crystals that were contained in each of the sample stacks.

Individual crystals and rock chips (0.05–0.5 mg) were re-packed into 5 mm deep 1.5 mm diameter wells in Al sample holders after irradiation, and fused sequentially without flux using a Spectra Physics 25 Watt argon-ion laser, generally in a single step at 15 W. For a biotite step-heating analysis (ID-47), the laser output was incrementally increased from 50 mW to > 10 W. Argon isotope analyses were carried out in static mode on an MAP 216 (Baur–Signer source) mass spectrometer, following two-stage gas purification through a liquid nitrogen-cooled glass cold finger, and SAES Zr–Al getters. Procedural blanks were measured between every fifth sample, typically ranging from 4×10^{-14} ccSTP at masses 36 and 39 to 3×10^{-12} cc STP at mass 40. Instrumental mass discrimination corrections are based on air pipette analyses and made up 1.008 per atomic mass unit during this measurement series. Ages were calculated with the decay constants of Steiger and Jäger (1977). Analytical uncertainties are quoted as 1σ, and include the uncertainties of peak signals, blank and monitor measurements. Mean apparent ages are weighted by the inverse variance (Taylor, 1982) and isochron ages and initial ^{40}Ar/^{36}Ar ratios are calculated according to York (1969).

References

Aceñolaza, F.G., Toselli, A.J., Durand, F.R., 1975. Estratigrafía y Paleontología de la región del Hombre Muerto, provincia de Catamarca, Argentina. 1er Congreso de Paleontología y Biostratigrafía, Actas I, 109–123.

Aceñolaza, F.G., Miller, H., Toselli, A.J., 1988. The Puncoviscana Formation (Late Precambrian-Early Cambrian): sedimentology, tectonometamorphic history and age of the oldest rocks of NW Argentina. Lecture Notes in Earth Sciences 17, 25–37.

Adelmann, D., 1997. Thrust tectonic controls on Late Tertiary sedimentation patterns in the Salar de Antofalla area (NW Argentina). I Congreso Latinoamericano de Sedimentología, Sociedad Venezolana de Geólogos, Memorias 1, 7–13.

Adelmann, D. in preparation Känozoische Beckenentwicklung in der südlichen Puna am Beispiel des Salar de Antofalla (NW-Argentinien). Doctoral thesis, Freie Universität Berlin.

Adelmann, D., Görler, K., 1998. Basin development in the Southern Puna: sedimentary record from the Salar de Antofalla area, NW Argentina. X Congreso Latinoamericano de Geología, Actas I, 26.

Allmendinger, R.W., Gubbels, T., 1996. Pure and simple shear plateau uplift, Altiplano-Puna, Argentina and Bolivia. Tectonophysics 259, 1–14.

Allmendinger, R.W., Ramos, V.A., Jordan, T.E., Palma, M., Isacks, B.L., 1983. Paleogeography and Andean structural geometry, northwest Argentina. Tectonics 2, 1–16.

Allmendinger, R.W., Jordan, T.E., Kay, S.M., Isacks, B.L., 1997. The evolution of the Altiplano-Puna Plateau of the Central Andes. Earth and Planetary Science Annual Review 25, 139–174.

Alonso, R.N., 1992. Estratigrafía del Cenozoico de la cuenca Pastos Grandes (Puna Salteña) con énfasis en la Formación Sijes y sus boratos. Revista de la Asociación Geológica Argentina 47, 189–199.

Alonso, R.N., Gutiérez, R., 1986. Litoestratigrafía del Neógeno terminal, Puna sudoriental Argentina. Revista del Instituto de Ciencias Geológicas 6, 29–47.

Alonso, R.N., Jordan, T.E., Tabutt, K.T., Vandervoort, D.S., 1991. Giant evaporite belts of the Neogene central Andes. Geology 19, 401–404.

Bahlburg, H., 1990. The Ordovician basin in the Puna of NW Argentina and N Chile: Geodynamical evolution from back-arc to foreland basin. Geotektonische Forschungen 75, 1–107.

Barazangi, M., Isacks, B.L., 1976. Spatial distribution of earthquakes and subduction of the Nazca Plate beneath South America. Geology 4, 686–692.

Benjamin, M.T., Johnson, N.M., Naeser, S.W., 1987. Recent rapid uplift in the Bolivian Andes: Evidence from fission-track dating. Geology 15, 680–683.

Cahill, T., Isacks, B., 1992. Seismicity and shape of the subducted Nazca plate. Journal of Geophysical Research 97, 17503–17529.

Christie-Blick, N., Biddle, K.T., 1985. Deformation and basin formation along strike-slip faults. In: Biddle, K.T., Christie-Blick, N. (Eds.), Strike-slip Deformation, Basin Formation and Sedimentation. Society of Economic Paleontologists and Mineralogists, Special Publication, 37, pp. 1–34.

Clayton, R., Mayeda, T., 1963. The use of bromine pentafluoride in the extraction of oxygen from oxides and silicates for isotopic analysis. Geochimica et Cosmochimica Acta 27, 43–52.

Coira, B., Pezzutti, N.E., 1976. Vulcanismo Cenozoico en el ámbito de la Puna catamarqueña. Revista Asociación Geológica Argentina 31 (1), 33–52.

Coira, B., Davidson, J., Mpodozis, C., Ramos, V.A., 1982. Tectonic and magmatic evolution of the Andes of northern Argentina and Chile. Earth Science Review 18, 303–332.

Coira, B., Kay, S.M., Viramonte, J., 1993. Upper Cenozoic magmatic evolution of the Argentine Puna—A model for changing subduction geometry. International Geology Review 35, 677–720.

Crough, S.T., 1983. Apatite fission-track dating of erosion in the eastern Andes, Bolivia. Earth Planetary Science Letters 64, 397–397.

Davidson, J.P., Harmon, R.S., Wörner, W., 1991. The source of Andean magmas; some considerations. In: Harmon, R.S., Rapela, C. (Eds.), Andean Magmatism and its Tectonic Setting. Geological Society of America Special Paper 265, 233–243.

De Silva, S.L., 1989. Altiplano-Puna volcanic complex of the central Andes. Geology 17, 1102–1106.

Döbel, R., Friedrichsen, H., Hammerschmidt, K., 1992. Implication of $^{40}Ar/^{39}Ar$ dating of early Tertiary volcanic rocks from the North Chilean Precordillera. Tectonophysics 202, 55–81.

Donato, E., 1987. Características estructurales del sector occidental de la Puna Salteña, Instituto Boliviano del Petróleo, v. Diciembre pp. 89–99.

Duffield, W.A., Dalrymple, G.B., 1990. Taylor Creek rhyolite of New Mexico, a rapidly emplaced field of domes and flows. Bulletin of Volcanology 52, 475–487.

Francis, P.W., Hawkesworth, C.J., 1994. Late Cenozoic rates of magmatic activity in the Central Andes and their relationships to continental crust formation and thickening. Journal of the Geological Society 151, 845–854.

Francis, P.W., Sparks, R.S.J., Hawkesworth, C.J., Thorpe, R.S., Pyle, D.M., Tait, S.R., Mantovani, M.S., McDermott, F., 1989. Petrology and geochemistry of volcanic rocks of the Cerro Galán caldera, northwest Argentina. Geological Magazine 126, 515–547.

Green, T.H., 1982. Anatexis of mafic crust and high pressure crystallization of andesite. In: Thorpe, R.S. (Ed.), Andesites: Orogenic Andesites and Related Rocks. Wiley, New York, pp. 465–487.

Günther, A., Haschke, M., Reutter, K-J., Scheuber, E., 1998. Kinematic evolution and structural geometry of the Chilean Precordillera (21.5-23°S): inversional tectonics in the Late Cretaceous-Paleogene magmatic arc. Terra Nostra 98/1.

Hawkesworth, C., 1979. $^{143}Nd/^{144}Nd$, $^{87}Sr/^{86}Sr$ and trace element characteristics of magmas along destructive plate margins. In: Atherton, M.P., Tarney, J. (Eds.), Origin of Granite Batholiths: Geochemical Evidence. Shiva, Nantwich, pp. 76–89.

Hérail, G., Soler, P., Bonhomme, M.G., Lizeca, J.L., 1993. Evolution géodynamique de la transition entre l'Altiplano et la Cordillère orientale au nord d'Oruro (Bolivie)—Implications sur le déroulement de l'orogénèse andine. Comptes Rendus de l'Académie des Sciences de Paris 317, 515–522.

Hunter, R.E., 1977. Basic types of stratification in small aeolian dunes. Sedimentology 24, 361–387.

Huene von, R., Corvalán, J., Flueh, E.R., Hinz, K., Korstgard, J., Ranero, C.R., Weinrebe, W., CONDOR scientists, 1997. Tectonic control of the subducting Juan Fernández Ridge on the Andean margin near Valparaíso, Chile. Tectonics 16, 474–488.

Isacks, B.L., 1988. Uplift of the central Andes and bending of the Bolivian orocline. Journal of Geophysical Research 93, 3211–3231.

James, D.E., 1971. Plate-tectonic model for the evolution of the central Andes. Geological Society America Bulletin 82, 3325–3346.

Jordan, T.E., Alonso, R.N., 1987. Cenozoic stratigraphy and basin tectonics of the Andes Mountains, 20°–28° south latitude. American Association of Petroleum Geologists Bulletin 71 (1), 49–64.

Jordan, T.E., Gardeweg, P.M., 1989. Tectonic evolution of the late Cenozoic central Andes (20°–33°S). In: Ben-Avraham, Z. (Ed.), The Evolution of the Pacific Ocean Margins. Oxford University Press, New York, pp. 193–207.

Kay, S., Mahlburg, Maksaev, V., Moscoso, R., Mpodozis, C., Nasi, C., Gordillo, C.E., 1988. Tertiary Andean magmatism in Chile and Argentina between 28°S and 33°S: Correlation of magmatic chemistry with a changing Benioff zone. Journal of South American Earth Science 1, 21–38.

Kay, S., Mahlburg, Mpodozis, C., Ramos, V., Munizaga, F., 1991. Magma source variations for mid-late Tertiary magmatic rocks associated with a shallowing subduction zone and a thickening crust in the central Andes (28 to 33°S). Geological Society of America Special Paper 265, 113–136.

Kay, S., Mahlburg, Coira, B., Viramonte, J., 1994a. Young mafic back arc volcanic rocks as indicators of continental lithospheric delamination beneath the Argentine Puna plateau, central Andes. Journal of Geophysical Research 99, 24,323–24,339.

Kay, S., Mahlburg, Mpodozis, C., Tittler, A., Cornejo, P., 1994b. Tertiary magmatic evolution of the Maricunga mineral belt in Chile. International Geology Review 36, 1079–1112.

Kay, S., Mahlburg, Coira, B., Mpodozis, C., 1997. Southern Central Volcanic Zone arc and back-arc mafic magmas: signals of Andean lithospheric processes (27°S to 25°S). VIII Congreso Geológico Chileno, Actas III, 1656–1660.

Kraemer, B., 1999. Eine geochemische Traverse quer zum mittelmio-

zänen magmatischen Bogen im südlichen Bereich der Zentralen Vulkanischen Zone der Anden (ZVZ, 25°–26°30′S, 67°30′–69°W). Unpublished Doctoral thesis. Freie Universität Berlin (174 pp.).

Lamb, S., Hoke, L., Kennan, L., Dewey, J., 1997. Cenozoic evolution of the Central Andes in Bolivia and northern Chile. In: Burg, J.-P., Ford, M. (Eds.), Orogeny through time, Geological Society Special Publication, 121, pp. 237–264.

Lanphere, M.A., Dalrymple, G.B., Fleck, R.J., Pringle, M.S., 1990. Intercalibration of mineral standards for K-Ar and ^{40}Ar/^{39}Ar measurements. EOS 71, 1658.

Le Maitre, R.W. (Ed.), 1989. A Classification of Igneous Rocks and Glossary of Terms. Blackwell, Oxford (193 pp.).

Marrett, R.A., Allmendinger, R.W., Alonso, R.N., Drake, R.E., 1994. Late Cenozoic tectonic evolution of the Puna Plateau and adjacent foreland, northwestern Argentine Andes. Journal of South American Earth Sciences 7 (2), 179–207.

Masek, J.G., Isacks, B.L., Guffels, T.L., Fielding, E.J., 1994. Erosion and tectonics at the margins of continental plateaus. Journal of Geophysical Research 99, 13941–13956.

Mpodozis, C., Cornejo, P., Kay, S.M., Tittler, A., 1995. La Franja de Maricunga: síntesis de la evolución del frente volcánico Oligoceno-Mioceno de la zona sur de los Andes Centrales. Revista Geológica de Chile 21, 273–313.

Naranjo, J.A., Cornejo, P., 1992. Hoja Salar de la Isla. Servicio Nacional de Geología y Minería, Carta Geológica de Chile 12.

Palma, M.A., Parrica, P.D., Ramos, V.A., 1986. El granito Archibarca: Su edad y significado tectónico, Provincia Catamarca. Revista de la Asociación Geológica Argentina XLI (34), 414–419.

Pardo-Casas, F., Molnar, P., 1987. Relative motion of the Nazca (Farallón) and South American plates since Late Cretaceous time. Tectonics 6, 233–246.

Pichler, H., Zeil, W., 1972. The Cenozoic rhyolite-andesite association of the Chilean Andes. Bulletin Volcanology 35, 424–452.

Pilger Jr., R.H., 1984. Cenozoic plate kinematics, subduction and magmatism: South American Andes. Journal of the Geological Society of London 141, 793–802.

Rapp, R.P., Watson, E.B., Miller, C.F., 1991. Partial melting of amphibolite/eclogite and the origin of Archean trondhjemites and tonalites. Precambrian Research 51, 1–25.

Reutter, K.J., Giese, P., Götze, H.J., Scheuber, E., Schwab, K., Schwarz, G., Wigger, P., 1988. Structures and crustal development of the Central Andes between 21° and 25°S. In: Bahlburg, H. (Ed.), The Southern Central Andes (Contributions to structure and evolution of an active continental margin). Lecture Notes in Earth Sciences 17, 231–261.

Salfity, J.A., 1985. Lineamentos transversales al rumbo Andino en el Noroeste Argentino. IV Congreso Geológico Chileno, Actas II, 119–137.

Salfity, J.A., Gorustovich, S.A., Moya, M.C., Amengual, R., 1984. Marco tectónico de la sedimentación y efusividad Cenozoicas en la Puna Argentina. VII Congreso Geológico Argentino, Actas I, 539–554.

Schreiber, U., Schwab, K., 1991. Geochemistry of Quaternary shoshonic lavas related to the Calama-Olacapato-El Toro Lineament, NW Argentina. Journal of South American Earth Sciences 4, 73–85.

Segerstrom, K., Turner, J.C.M., 1972. A conspicious flexure in regional structural trend in the Puna of northwestern Argentina. U.S. Geological Survey Prof. Paper 800-B, 205–209.

Soler, P., Jiménez, N., 1993. Magmatic constraints upon the evolution of the Bolivian Andes since the late Oligocene times. 2nd International Conference Andean Geodynamics, pp. 447–451.

Somoza, R., 1998. Updated Nazca (Farallon)—South America relative motions during the last 40 My: implications for mountain building in the central Andean region. Journal of South American Earth Sciences 11, 211–215.

Steiger, R.H., Jäger, E., 1977. Subcommission on Geochronology: convention on the use of decay constants in geo- and cosmochronology. Earth and Planetary Science Letters 36, 359–362.

Steinmann, G., 1929. Geologie von Peru. Karl Winter, Heidelberg (448 pp.).

Taylor, J.R., 1982. An Introduction to Error Analysis. University Science Books, Mill Valley, California (270 pp.).

Turner, J.C., 1960. Estratigrafia del Nevado de Cachi y sector al oeste. Acta Geológica Lilloana 3, 191–226.

Vandervoort, D.S., Jordan, T.E., Zeitler, P.K., Alonso, R.N., 1995. Chronology of internal drainage development and uplift, southern Puna plateau, Argentine central Andes. Geology 23 (2), 145–148.

Voss, R., Görler, K., Kraemer, B., van den Bogaard, P., 1996. Neue Daten zur paläozoischen und mesozoischen Paläogeographie in der südlichen Puna (NW-Argentinien). Terra Nostra 8/96, 147.

Voss, R., in preparation. Känozoische Stratigraphie, Sedimentologie und Tektonik in der Umgebung des südlichen Salar de Antofalla, NW Argentinien. Doctoral thesis. Freie Universität Berlin.

Whitman, D., Isacks, B.L., Kay, S. Mahlburg, 1996. Lithospheric structure and along-strike segmentation of the Central Andean plateau: topography, tectonics and timing. Tectonophysics 259, 29–40.

Wigger, P., 1988. Seismicity and crustal structure of the Central Andes. Bahlburg, H. (Ed.), The Southern Central Andes (Contributions to structure and evolution of an active continental margin). Lecture Notes in Earth Sciences, 17, 209–229.

Willner, A.P., Lottner, U.S., Miller, H., 1987. Early Paleozoic structural development in the NW Argentine basement of the Andes and its implication for geodynamic reconstruction. In: McKenzie, G.D. (Ed.), Gondwana Six; Structure, Tectonics, and Geophysics. Geophysical Monographs, 40, 229–239.

Wolf, M.B., Wyllie, P.J., 1994. Dehydration-melting of amphibolite at 10 kbar: the effects of temperature and time. Contributions to Mineralogy and Petrology 115, 369–383.

Woodcock, N.H., Fischer, M., 1986. Strike-slip duplexes. Journal of Structural Geology 8 (7), 725–735.

York, D., 1969. Least squares fitting of a straight line with correlated errors. Earth and Planetary Science Letters 5, 320–324.

Zuleger, E., Erzinger, J., 1988. Determination of the REE and Y in silicate materials with ICP-AES. Fresenius Zeitschrift für Analytische Chemie 332, 140–143.